Relative Importance of High-Latitude Local and Long-Range Transported Dust to Arctic Ice Nucleating Particles and Impacts on Arctic Mixed-Phase Clouds

Yang Shi[1], Xiaohong Liu[1], Mingxuan Wu[2], Xi Zhao[1], Ziming Ke[1], and Hunter Brown[1]

[1]Department of Atmospheric Sciences, Texas A&M University, College Station, TX, USA
[2]Atmospheric Sciences and Global Change Division, Pacific Northwest National Laboratory, Richland, WA, USA

Correspondence to: Xiaohong Liu (xiaohong.liu@tamu.edu)

Abstract. Dust particles, serving as ice nucleating particles (INPs), may impact the Arctic surface energy budget and regional climate by modulating the mixed-phase cloud properties and lifetime. In addition to long-range transport from low latitude deserts, dust particles in the Arctic can originate from local sources. However, the importance of high latitude dust (HLD) as a source of Arctic INPs (compared to low latitude dust (LLD)) and its effects on Arctic mixed-phase clouds are overlooked. In this study, we evaluate the contribution to Arctic dust loading and INP population from HLD and six LLD source regions by implementing a source-tagging technique for dust aerosols in version 1 of the US Department of Energy's Energy Exascale Earth System Model (E3SMv1). Our results show that HLD is responsible for 30.7% of the total dust burden in the Arctic, whereas LLD from Asia and North Africa contribute 44.2% and 24.2%, respectively. Due to its limited vertical transport as a result of stable boundary layers, HLD contributes more in the lower troposphere, especially in boreal summer and autumn when the HLD emissions are stronger. LLD from North Africa and East Asia dominates the dust loading in the upper troposphere with peak contributions in boreal spring and winter. The modeled INP concentrations show a better agreement with both ground and aircraft INP measurements in the Arctic when including HLD INPs. The HLD INPs are found to induce a net cooling effect (-0.24 W m^{-2} above 60°N) on the Arctic surface downwelling radiative flux by changing the cloud phase of the Arctic mixed-phase clouds. The magnitude of this cooling is larger than those induced by North African and East Asian dust (0.08 and -0.06 W m^{-2}, respectively), mainly due to different seasonalities of HLD and LLD. Uncertainties of this study are discussed, which highlights the importance of further constraining the HLD emissions.

1 Introduction

The Arctic has experienced long-term climate changes, including rapid warming and shrinking in sea ice extent. Arctic mixed-phase clouds (AMPCs), which occur frequently throughout the year, strongly impact the surface and atmospheric energy budget and are one of the main components driving the Arctic climate (Morrison et al., 2012; Shupe and Intrieri, 2004; Tan and Storelvmo, 2019). The AMPCs lifetime, properties, and radiative effects are closely connected to the primary ice formation process, as the formed ice crystals grow at the expense of cloud liquid droplets due to the lower saturation vapor pressure with respect to ice than that to liquid water (so-called Wegener-Bergeron-Findeisen process or, in short, WBF process; Liu et al., 2011; M. Zhang et al., 2019). Large ice crystals with higher fall speeds than liquid droplets can readily initiate precipitation and further deplete cloud liquid through the riming process. All these processes can also interact with each other nonlinearly and impact the phase partitioning of mixed-phase clouds (Tan and Storelvmo, 2016).

Primary ice formation in mixed-phase clouds only occurs heterogeneously with the aid of ice nucleating particles (INPs). According to Vali et al. (1985), the heterogeneous ice nucleation is classified into four different modes: through the collision of an INP particle with supercool liquid droplet (contact freezing), by an INP particle immersed in a liquid droplet (immersion freezing), when the INP particle also serves as a cloud condensation nucleus (condensation freezing), or by the direct deposition of water vapor to a dry INP particle (deposition nucleation). The immersion freezing is usually treated together with condensation freezing in models, as instruments cannot distinguish between them (Vali et al., 2015). This immersion/condensation freezing is generally thought to be the most important ice nucleation mode in the mixed-phase clouds (de Boer et al., 2011; Prenni et al., 2009; Westbrook and Illingworth, 2013). It remains a significant challenge to

characterize the INP types and concentrations, partially because only a very small fraction of aerosols can serve as INPs (DeMott et al., 2010). This is especially the case for the clean environment in the Arctic. Therefore, the potential sources and amounts of Arctic INPs are still largely unknown.

Mineral dust aerosols are identified as one of the most important types of INPs in the atmosphere due to their high ice nucleation efficiency (DeMott et al., 2003; Hoose and Möhler, 2012; Murray et al., 2012; Atkinson et al., 2013) and their abundance in the atmosphere (Kinne et al., 2006). They are mainly emitted from arid and semi-arid regions located at low- to mid-latitudes, such as North Africa, the Middle East, and Asia. Observational studies found that LLD can be transported to the Arctic (Bory et al., 2003; VanCuren et al., 2012; Huang et al., 2015) and act as a key contributor to the Arctic INP population (Si et al., 2019). A modelling study also suggested that low latitude dust (LLD) has a large contribution to dust concentrations in the upper troposphere of the Arctic (Groot Zwaaftink et al., 2016), since LLD is usually lifted by convection and topography and then transported poleward following slantwise isentropes. This finding confirms the potential of LLD to serve as INPs in AMPCs. The impact of LLD INPs on clouds was further investigated by Shi and Liu (2019), who found that LLD INPs induce a net cooling cloud radiative effect in the Arctic, due to their impacts on cloud water path and cloud fraction.

Although LLD has attracted much of the attention in the past, it is recognized that 2–3% of the global dust emission is produced by local Arctic sources above 50°N (Bullard et al., 2016), which include Iceland (Arnalds et al., 2016; Dagsson-Waldhauserova et al., 2014; Prospero et al., 2012), Svalbard (Dörnbrack et al., 2010), Alaska (Crusius et al., 2011), and Greenland (Bullard and Austin, 2011). Groot Zwaaftink et al. (2016) found that high latitude dust (HLD) contributes 27% of the total dust burden in the Arctic. Different from LLD, most of the emitted HLD is restricted

79 at the lower altitudes in the Arctic, because of the stratified atmosphere in the cold environment
80 (Bullard, 2017; Groot Zwaaftink et al., 2016).

81 It is also noted that HLD is likely an important source to the observed INPs in the Arctic,
82 especially during the warm seasons. For example, Irish et al. (2019) suggested that mineral dust
83 from Arctic bare lands (likely eastern Greenland or north-western continental Canada) is an
84 important contributor to the INP population in the Canadian Arctic marine boundary layer during
85 summer 2014. Attempts have been made to quantify the ice nucleating ability of HLD. Paramonov
86 et al. (2018) found that the Icelandic glaciogenic silt had a similar ice nucleating ability as LLD at
87 temperatures below -30 °C. Similarly, Sanchez-Marroquin et al. (2020) suggested that the ice
88 nucleating ability of aircraft-collected Icelandic dust samples is slightly lower but comparable with
89 that of the LLD. Some other studies also noticed that HLD can act as efficient INPs at warm
90 temperatures. As early as the 1950s, the airborne dry dust particles from permafrost ground at
91 Thule, Greenland, were found to nucleate ice at temperatures as warm as -5 °C (Fenn and
92 Weickmann, 1959). This is corroborated by a more recent study which investigated the glacial
93 outwash sediments in Svalbard and ascribed the remarkably high ice nucleating ability to the
94 presence of soil organic matter (Tobo et al., 2019).

95 Despite their potential importance, HLD sources are largely underestimated or even omitted in
96 global models (Zender et al., 2003). Fan (2013) noticed that the autumn peak in measured surface
97 dust concentrations at Alert was underestimated by the model, likely due to a lack of local dust
98 emission. Similarly, Shi and Liu (2019) also mentioned that the distinction of simulated and
99 satellite retrieved dust vertical extinction in the Arctic became larger near the surface.

100 In this study, we account for the HLD dust emission by replacing the default dust emission
101 scheme (Zender et al., 2003) with the Kok et al. (2014a, b) scheme in the Energy Exascale Earth

System Model version 1 (E3SMv1). We further track explicitly the dust aerosols emitted from the Arctic (HLD) and six major LLD sources using a newly developed source-tagging technique in E3SMv1. The objectives of this study are to (1) examine the source attribution of the Arctic dust aerosols in the planetary boundary layer and in the free troposphere; (2) examine the contribution of dust from various sources to the Arctic dust INPs; and (3) quantify the subsequent influence of dust INPs from various sources on the Arctic mixed-phase cloud radiative effects. We are particularly interested in the relative importance of local HLD versus long-range transported LLD.

The paper is organized as follows. The E3SMv1 model and experiments setup are introduced in Section 2. Section 3 presents model results and comparisons with observations. The uncertainties are discussed in Section 4, and Section 5 summarizes the results.

2 Methods

2.1 Model description and experiment setup

Experiments in this study are performed using the atmosphere component (EAMv1) of the U.S. Department of Energy (DOE) E3SMv1 model (Rasch et al., 2019). The model predicts number and mass mixing ratios of seven aerosol species (i.e., mineral dust, black carbon (BC), primary organic aerosol, secondary organic aerosol, sulfate, sea salt, and marine organic aerosol (MOA)) through a four-mode version of modal aerosol module (MAM4) (Liu et al., 2016; Wang et al., 2020). The four aerosol modes are Aitken, accumulation, coarse, and primary-carbon modes, while dust aerosols are carried in accumulation and coarse modes. Aerosol optical properties in each mode is parameterized following Ghan and Zaveri (2007). The dust optics used in this study are updated according to Albani et al. (2014).

EAMv1 includes a two-moment stratiform cloud microphysics scheme (MG2) (Gettelman and Morrison, 2015). We note the WBF process rate in EAMv1 is tuned down by a factor of 10, which results in more prevalent supercooled liquid water clouds in high latitudes than observations and many other global climate models (Y. Zhang et al., 2019; Zhang et al., 2020). In addition, the Cloud Layers Unified By Binormals (CLUBB) parameterization (Bogenschutz et al., 2013; Golaz and Larson, 2002; Larson et al., 2002) is used to unify the treatments of planetary boundary layer turbulence, shallow convection, and cloud macrophysics. Deep convection is treated by the Zhang and McFarlane (1995) scheme.

In EAMv1, the heterogeneous ice nucleation in mixed-phase clouds follows the classical nucleation theory (CNT) (Hoose et al., 2010; Y. Wang et al., 2014). CNT holds the stochastic hypothesis, which treats the ice nucleation process as a function of time. Immersion/condensation, contact, and deposition nucleation on dust and BC are treated in the CNT scheme. More details about CNT parameterization are provided in Text S2.1 in the Supplement.

The experiments we conducted for this study are shown in Table 1. For the control experiment (hereafter CTRL), the EAMv1 was integrated from July 2006 to the end of 2011 at 1° horizontal resolution and 72 vertical layers. The first six months of the experiment were treated as model spin-up and the last five-year results were used in analyses. The horizontal wind components were nudged to the MERRA2 meteorology with a relaxation timescale of 6 hours (Zhang et al., 2014). In addition to CTRL, we conducted three sensitivity experiments to investigate the INP effect of dust from major source regions. In these sensitivity experiments, heterogeneous ice nucleation in the mixed-phase clouds by dust from local Arctic sources, North Africa, and East Asia is turned off (i.e., noArc, noNAf, and noEAs, respectively). The other settings of these three experiments are identical to CTRL. Analyses related to the sensitivity experiments are provided in Section 3.4.

2.2 Dust emission parameterization and source-tagging technique

Dust emission in the default EAMv1 is parameterized following Zender et al. (2003) (Z03), which uses semi-empirical dust source functions to address the spatial variability in soil erodibility. The HLD emission is omitted in the Z03 scheme, since it was thought to be dubious (Zender et al., 2003). In this study, we replaced the Z03 scheme with another dust emission parameterization (Kok et al., 2014a, b) (K14) that avoids using a source function (see more details about K14 in Text S1). The K14 scheme is able to produce the HLD emission over Iceland, the Greenland coast, Canada, Svalbard, and North Eurasia (Figure 1a). Furthermore, to address the overestimation in dust emission in clay size ($< 2\ \mu$m diameter) (Kok et al., 2017), we changed the size distribution of emitted dust particles from Z03 to that based on the brittle fragmentation theory (Kok, 2011). 1.1% of the total dust mass is emitted to the accumulation mode and 98.9% of that is emitted to the coarse mode based on the brittle fragmentation theory, whereas the fractions are 3.2% and 96.8%, respectively in Z03.

To quantify the source attribution of dust, we implemented a dust source-tagging technique in EAMv1. This modeling tool was previously applied to BC (H. Wang et al., 2014; Yang et al., 2017b), sulfate (Yang et al., 2017a), and primary organic aerosol (Yang et al., 2018) in the Community Atmosphere Model version 5 (CAM5). In this method, dust emission fluxes from different sources are assigned to separate tracers and transport independently, so that dust originating from different sources can be tracked and tuned separately in a single model experiment. As shown in Figure 1a, dust emissions from 7 source regions are tagged: Arctic (Arc; above 60°N, HLD source), North America (NAm), North Africa (NAf), Central Asia (CAs), Middle East and South Asia (MSA), East Asia (EAs), and rest of the world (RoW). The Arctic source is further divided into four sub-sources: Alaska (Ala), North Canada (NCa), Greenland and Iceland (GrI),

and North Eurasia (NEu) (Figure S1), which are used in the analysis of INP sources in Section 3.3. RoW represents the three major dust sources in the Southern Hemisphere (South America, South Africa, and Australia), along with very low emissions from Europe and the Antarctic.

The global dust emission for CTRL is 5640 Tg yr^{-1}, which is tuned so that the global average dust aerosol optical depth (DOD) is 0.031. This is within the range of the observational estimate (0.030±0.005) by Ridley et al. (2016). To maintain the magnitude of the global averaged DOD, our tuned global dust emission exceeds the range of the AeroCom (Aerosol Comparisons between Observations and Models) models (500 to 4400 Tg yr^{-1}; Huneeus et al., 2011), likely due to a short lifetime caused by too strong dust dry deposition at the bottom layer near the dust source regions in EAMv1 (Wu et al., 2020). It is also about 2000 Tg yr^{-1} higher than the previous EAMv1 studies (Shi and Liu, 2019; Wu et al., 2020), because we distribute less dust mass into the accumulation mode and more dust mass into the coarse mode based on Kok (2011). The HLD emission is further tuned up by 10 times so that it accounts for 2.6% (144 Tg yr^{-1}) of the global dust emission (Figure 1b), which is comparable with the recent estimates of 2-3% above 50°N by Bullard et al. (2016) and of 3% above 60°N by Groot Zwaaftink et al. (2016). The majority of global dust emission is contributed from North Africa (51.9%, 2929 Tg yr^{-1}) and Asia (37.7%, 2124 Tg yr^{-1}), with Asian emissions composed of MSA (20.2%, 1140 Tg yr^{-1}), EAs (10.9%, 613 Tg yr^{-1}), and CAs (6.6%, 371 Tg yr^{-1}). NAm has a weak dust emission of 33.4 Tg yr^{-1} that only contributes 0.6% to the global emission, while the RoW has a combined contribution of 7.3% (410 Tg yr^{-1}). In addition, the seasonal variations between HLD and LLD emissions are different - the HLD (Arctic) source is more active in late summer and autumn, while the LLD sources (e.g., NAf, MSA, EAs) peak in spring and early summer (Figure 1c).

3 Result

3.1 Model validation

To evaluate the model performance in simulating the dust cycle, we compare the model predictions with measured aerosol optical depth (AOD), dust surface concentrations, and dust deposition fluxes from global observation networks (Figure 2). We select and process the level 2.0 AOD data (2007-2011) at 40 "dust-dominated" AErosol RObotic NETwork (AERONET; Holben et al., 1998) stations following Kok et al. (2014b). We note that the AERONET AOD measurements are biased towards clear-sky conditions due to the cloud-screening procedure (Smirnov et al., 2000). For dust surface concentrations, we use the same measurements at 22 sites, which Huneeus et al. (2011) used for the AeroCom comparison, and further extend the dataset with measurements at three high latitude stations: Heimaey (Prospero et al., 2012), Alert (Sirois and Barrie, 1999), and Trapper Creek (Interagency Monitoring of Protected Visual Environments; IMPROVE). It is noted that the measurements at Trapper Creek only include dust particles smaller than 2.5 μm and are only compared with simulated dust concentrations at the same size range. All other concentration measurements capture dust particles below 40 μm and are compared with simulated dust over the whole size range (< 10 μm). The dust deposition fluxes dataset, which including 84 stations, is also the same as Huneeus et al. (2011). The locations of the observation network are shown in Figure 2d, with the AOD data taken close to source regions and the dust surface concentrations and deposition fluxes measured at relatively remote regions. The Pearson correlation coefficient (r) are provided for each comparison. We note that the comparisons are subject to representative biases caused by comparing an observational station with a global model grid point (with a horizontal resolution of ~ 100 km). The comparisons of dust concentration and

deposition flux also have systematic errors because the measurements were for a different time period than that of the model simulation.

In general, the three comparisons indicate that our CTRL simulation is capable of capturing the global dust cycle in both near the source and remote regions. As shown in Figure 2a, the modeled AOD is within a factor of two of the observations over most of the stations. The correlation of the AOD comparison is 0.73, which is comparable to the best performing simulation ($r = 0.72$) in Kok et al. (2014b). Our model also does a fairly good job in simulating the dust surface concentrations (Figure 2b) and produces a correlation coefficient of 0.84. For the three high latitude sites, the model shows moderate underestimation at Heimaey and Trapper Creek and large positive bias at Alert (see discussion below). The correlation coefficient for simulated dust deposition fluxes ($r = 0.48$) is also within the range of the AeroCom comparisons (0.08 to 0.84) in Huneeus et al. (2011). The model results over most of the sites are within one order of magnitude difference, except at the polar regions. In particular, the model overestimates the dust deposition flux in Greenland (red triangles in Figure 2c and 2d) by around two orders of magnitude, likely due to too strong local emissions simulated near the coast of Greenland (Figure 1a).

The seasonal cycle of dust surface concentrations at the three Arctic stations (Heimaey, Alert, and Trapper Creek) are shown in Figure 3, along with the contribution from seven tagged sources. The simulated dust concentrations at Heimaey are dominated by HLD and agree well with the observation in late summer and autumn (Figure 3a). Its annual-averaged low bias shown in Figure 2b mainly comes from the springtime, when Prospero et al. (2012) found the observed dust are related to dust storms in Iceland, indicating a possible underestimation in the simulated Icelandic dust during this time. The HLD also dominates the surface dust concentrations at Alert (Figure 3b), leading to a large overestimation from June to August in our simulation, which possibly implies a

high bias and wrong seasonal cycle of HLD emission over Greenland and North Canada. The Trapper Creek station is instead dominated by LLD from East Asia and shows an underestimation for most of the year. It is noted that we only include fine dust (diameter < 2.5 μm) for the comparison at Trapper Creek. Larger size range is likely to be more influenced by HLD sources. The low bias here, especially that during the autumn, can be related to the missing of local emissions from the coast of Southern Alaska (Figure 1a) that occurs most frequently in autumn (Crusius et al., 2011). An underestimation of the transport from Saharan dust may also contribute slightly, as the influence from Saharan dust is found during mid-May at Trapper Creek (Breider et al., 2014).

The simulated Arctic dust vertical profiles are also compared with the measured dust concentrations during the Arctic Research of the Composition of the Troposphere from Aircraft and Satellites (ARCTAS) flight campaign (Figure 4) (Jacob et al., 2010). The ARCTAS campaign was conducted over the North American Arctic in April and July 2008. The simulated profiles are averaged over the regions where the aircraft flew, in accordance with Groot Zwaaftink et al. (2016). In April, the model does a good job in capturing the Arctic dust vertical profiles (Figure 4a). However, in July, the model underestimates dust by a factor of 2 to 5 between 3 and 10 km (Figure 4b). It also shows an overestimation near the surface in July, which agrees with the surface concentrations comparison at Alert station (Figure 3b). The underestimation in the upper troposphere and overestimation near the surface likely imply a too weak vertical transport of HLD in the North American Arctic in summertime. The high bias in the upper troposphere may also be related to an underrepresentation of LLD transport.

Finally, we evaluate the simulated dust extinction against the Cloud-Aerosol Lidar and Infrared Pathfinder Satellite Observation (CALIPSO) retrieval (Luo et al., 2015a, b; Yang et al., 2022),

which includes nighttime dust extinction for the period of 2007 to 2009. This data set has improvements in dust separation from other aerosol types and thin dust layer detection in the Arctic compared to the standard Cloud-Aerosol Lidar with Orthogonal Polarization (CALIOP) Level 2 product (Winker et al., 2013). To make an apple-to-apple comparison, the modeled dust extinction is sampled along the CALIPSO tracks and screened by cloud fraction (Wu et al., 2020). For this comparison, we only use the first three years (2007 to 2009) of the CTRL simulation to be consistent with the observation period. Overall, the model does a good job in capturing the Arctic dust extinction vertical profiles (Figure 5). We notice that the simulated dust extinction is lower than CALIPSO retrievals at the upper troposphere in summer, which agrees with the ARCTAS comparisons. The simulated dust extinction also shows a consistent underestimation in springtime (MAM) and a near surface underestimation in wintertime (MAM). Since the Arctic is mostly covered by ice and snow in these two seasons, the impacts of HLD are expected to be limited and the low biases are most likely due to the underprediction of LLD transport. The near surface underestimation in DJF may indicate a too weak LLD transport in the lower troposphere (e.g., the transport of dust emitted from Central Asia; see Figure 7 and the corresponding discussions in Section 3.2). Moreover, the HLD has a large contribution in the lower troposphere in boreal summer and autumn, which is consistent with its strong emission at that time. In contrast, LLD plays a more dominant role in the upper troposphere, where African dust contributes the most in the springtime and East Asian dust has a larger contribution in the other seasons.

Deleted: The Luo et al. (2015a, b)

Deleted: than

Deleted: CALIPSO

3.2 Arctic dust mass source attribution

Table 2 summarizes the relative contributions from individual sources to the total Arctic dust burden. The transport pathways can be identified from the dust burden spatial distribution for each source in Figure 6, while the relative contribution of each source to the total dust burden is shown

285 in Figure S2. We also calculate the regional burden efficiency for each source (Table S1), which
286 is defined as the mean contribution to the Arctic dust column burden divided by the corresponding
287 dust emission (H. Wang et al., 2014). This metric represents the sensitivity of Arctic dust loading
288 to per unit change of dust emission from each source (i.e., the poleward transport efficiency of
289 each source).

290 Our model results suggest that the HLD (Arc) is the largest contributor (30.7%) to the annual
291 mean Arctic dust burden among all the tagged sources. As shown in Figure 6a and Figure S2a, the
292 local dust is confined within the high latitudes, with the higher amounts and higher contributions
293 to the total dust burden near the sources in North Canada, coast of Greenland, and Iceland. The
294 interior of the Greenland ice sheet, with its higher elevations, is more influenced by LLD from
295 North Africa and East Asia than HLD (Figure S2c and S2f). This is due to the weak vertical
296 transport of local emissions in the Arctic (see more discussions below).

297 On the other hand, all LLD sources are responsible for 69.3% of the dust loading in the Arctic,
298 with considerable contributions from North Africa (24.2%) and Asia (in total 44.2%; EAs: 19.9%,
299 MSA: 11.5%, CAs: 12.8%), and minor contributions from NAm (0.1%) and RoW (nearly 0). The
300 North African dust is primarily transported westward to the Atlantic and southward to Sahel, with
301 a smaller fraction transported directly northward or northeastward across the Eurasia to the Arctic
302 (Figure 6c; Shao et al., 2011). The westward trajectory can also bring dust to the Arctic through
303 the Azores high (e.g., VauCuren et al., 2012), but this pathway is not clearly seen on Figure 6c
304 likely due to the strong wet removal process over the North Atlantic. As evident by the low
305 transport efficiency in Table S1, the significant contribution of the North African dust to the Arctic
306 dust burden is mainly due to its massive emission. However, this is not the case for EAs. The East
307 Asian dust is first lifted vertically by topography and convection (Shao et al., 2011) and is widely

spread over the Northern Hemisphere mid- and high-latitude regions through the westerly flow in the upper troposphere (Figure 6f). The high elevation of East Asian dust plumes results in weaker removal processes and thus an efficient poleward transport. As shown in Table S1, the annual transport efficiency of the East Asian dust is relatively high among the LLD sources, which is nearly three times larger than that of the North African dust. The poleward transport of dust from CAs and MSA both takes the pathway across Siberia (Figure 6d and 6e). The transport efficiency of the CAs dust is two times higher than that of the MSA dust (Table S1). This is attributed to CAs being closer to the Arctic and having less southward dust transport than MSA. Overall, the LLD from North Africa and Asia contributes more to the Eurasia and Pacific sector of the Arctic (Figures S2c to S2f). The impact of NAm dust is limited by its weak emission (Figure 6b), while dust emitted in the Southern Hemisphere (RoW) can hardly pass the equator (Figure 6g).

Earlier modeling studies (Breider et al., 2014; Groot Zwaaftink et al., 2016; Luo et al., 2003; Tanaka and Chiba, 2006) also quantify the relative contributions of dust from various regions to the Arctic dust loading. Among these studies, only Groot Zwaaftink et al. (2016) includes HLD. Our estimate about the HLD percent contribution is close to that from their study (27%). For LLD, our conclusion about the dominant role of African and Asian dust to the Arctic dust burden is also corroborated by these previous studies. However, the relative importance of African and Asian dust is uncertain. Based on our results, the Asian dust is responsible for 65% of the LLD transport to the Arctic, while the African dust only contributes 35%. Other studies find that 50% (Groot Zwaaftink et al., 2016; Luo et al., 2003; Tanaka and Chiba, 2006) to as much as 65% (Breider et al., 2014) of the LLD in the Arctic is attributed to North Africa. These discrepancies may be explained by the different dust emission and scavenging, dust size distribution, meteorological fields, and/or time periods for the model simulation. For example, the wet removal process is

Deleted: For example,

expected to have large discrepancies among different models, because of the large uncertainties in the model representation of clouds and precipitation. The different spatial distributions of dust emission due to the use of different emission parameterizations may also contribute to the discrepancies (e.g., North Africa dust in our study contributes slightly less (51.9%) to the global dust emission than the other studies (from 57% to 67%). Isotopic analysis (Bory et al., 2002, 2003) and case studies (Huang et al., 2015; Stone et al., 2005; VanCuren et al., 2012) have proved that both Asian and African dust can be transported to the Arctic. However, it remains unclear which of them contributes more to the Arctic dust loading due to the limited observational constraints.

HLD and LLD source regions also have very distinct vertical distributions in the Arctic. Figures 7a and 7b show the annual mean vertical profiles of Arctic dust concentrations from various sources and their percentage contributions, respectively. The Arctic dust in the lower atmosphere is dominated by the local source. HLD accounts for more than 30% of the Arctic dust concentrations below 800 hPa, with up to 85% contribution near the surface. However, the HLD contribution decreases rapidly with height and is less than 10% above 700 hPa. This is because the lower troposphere of the Arctic is more stratified than the mid- and low latitudes, which suppresses the vertical transport of HLD. The lower tropospheric stability (LTS) from the CTRL simulation and comparison with the MERRA2 reanalysis data are shown in Figure S3. The weak HLD vertical transport in the Arctic is also reported by previous studies (Groot Zwaaftink et al., 2016, Baddock et al., 2017; Bullard, 2017). Moreover, the LTS over the Arctic sea ice is much larger than that over open ocean surface (Schweiger et al., 2008), which may lead to a stronger vertical transport of HLD over open waters. This suggests that the vertical transport of HLD may change with the sea ice reduction in a warming future.

In contrast, LLD has a higher contribution in the mid- and upper troposphere than near the surface. Such a vertical distribution of LLD is consistent with Stohl (2006) and Groot Zwaaftink et al. (2016). As Stohl (2006) found, aerosols originating from the warm subtropics are transported poleward following the uplifted isentropes and the Arctic lower atmosphere is dominated by the near-impenetrable cold polar dome. Therefore, there is a slantwise lifting of low latitude aerosols during their poleward transport. NAf and EAs are the two key contributors to the Arctic dust vertical concentrations, each of which contributes up to one third of the total dust concentrations above 700 hPa. Dust emission from MSA also has a moderate contribution (15-20%) that increases gradually with height, while the contribution from CAs peaks at 700 to 800 hPa, indicating a lower altitude transport pathway than the EAs and MSA dust.

In addition, the Arctic dust undergoes a strong seasonal cycle (Table 2 and Figures 7c-j). Because of the strong local emissions (Figure 1c), about half of the Arctic dust burden in summer and autumn come from HLD, with more than 50% contribution of Arctic dust concentrations below 850 hPa in these two seasons. In contrast, LLD plays a dominant role in spring and winter. The North African dust has the largest contribution in spring, which accounts for about 45% of the total dust concentrations above 700 hPa. The East Asian dust is more important in the other three seasons. Due to its high emission height, the relative contribution from EAs tends to increase with height and reaches 30% to 50% of the total dust concentration above 500 hPa in summer, spring, and winter.

3.3 Immersion freezing on dust in the AMPCs

We are particularly interested in the contribution of various dust sources to the Arctic INP populations. Therefore, we compare the simulated INP concentrations with nine Arctic field measurements, which are summarized in Table 3. The modeled dust INP concentrations are

diagnosed from monthly averaged aerosol properties using the default CNT scheme and two empirical ice nucleation parameterizations, DeMott et al. (2015; hereafter as D15) and Sanchez-Marroquin et al. (2020; hereafter as SM20). The D15 parameterization, which is representative of Saharan and Asian desert dust, relates dust INP number concentrations to the number concentration of dust particles larger than 0.5 μm diameter and is found to produce the most reasonable LLD INP concentrations in EAMv1 (Shi and Liu, 2019). CNT and D15 are applied to LLD only and all the dust aerosols (LLD and HLD) in Figures 8a-b and Figures 8d-e, respectively. The SM20 parameterization, which is derived for the HLD Icelandic dust, describes the dust INP number concentrations as a function of surface active site density and total dust surface area. Considering the possibly different ice nucleation ability between HLD and LLD, we only applied the SM20 parameterization to HLD and the CNT and D15 parameterizations are still applied to LLD in Figures 8c and 8f, respectively. To account for the contributions from other aerosol types, we also calculate the INP concentrations from BC (Fig. 8g) and sea spray aerosol (SSA; includes MOA and sea salt) (Fig. 8h) following Schill et al. (2020; hereafter as Sc20) and McCluskey et al. (2018; hereafter as M18), respectively. More details about the ice nucleation parameterizations are provided in Text S2. We discuss the choice of dust ice nucleation schemes in Text S2.6 in the Supplement.

Overall, only including LLD as INPs results in up to four orders of magnitude underprediction compared to observations (Figures 8a and 8d), while taking into account the contribution from HLD greatly improves the model performance by increasing the simulated dust INP concentrations (Figures 8b, 8c, 8e, and 8f). The CNT parameterization produces 5 to 10 times more INP concentrations than the other two schemes at moderately cold temperatures (-22 to -28℃), while it has a significant underestimation of observed INP concentrations at warm temperatures (T > -

18℃) (also see Figure S4). D15 and SM20 agree well with each other in simulating HLD INPs, with SM20 producing slightly higher results than D15. Our modeling results also indicate that BC and SSA have much less contributions to INP than dust in all the nine field campaigns (Figure 8g and 8h).

A detailed analysis of sources of the INPs for the nine datasets based on modeling analyses and the corresponding observations in the literature are provided in Table 3. Modeling results indicate that HLD has larger contributions to the INPs for the campaigns conducted in summer and autumn than spring, in agreement with the observations. Also, ground-based measurements are more influenced by the nearby HLD sources, while LLD from EAs and NAf contributes more to the aircraft measurements.

Our modeling analyses about the INP sources agree well with the observational studies at Alert in spring 2016 and near Iceland in autumn 2014 (symbol "C" and "I" in Figure 8, respectively), while the model underestimates the observed INP concentrations in both cases. The low bias in dataset C indicates an underprediction in the long-range transport of Asian dust to the Arctic surface in springtime. The underestimation in dataset I is more likely due to the fact that some of the aircraft measurements were taken inside the Icelandic dust plumes (Sanchez-Marroquin et al., 2020), which cannot be resolved by the monthly mean model output and the coarse model horizontal resolution (1°). Such uncertainties exist in all the model-observation comparisons.

Some other comparisons in INP sources reveal the lack of marine and carbonaceous INPs in the model. The model results show a dominance of dust INPs in spring 2017 at Zeppelin and Oliktok Point (symbol "D" and "E" in Figure 8) and in Autumn 2004 at Utqiaġvik (symbol "H" in Figure 8), while the observational studies suggested the importance of marine sources at the first two locations and of carbonaceous aerosols at Utqiaġvik. Therefore, it is likely that the model

underestimates the contribution of MOA (Wilson et al., 2015; Zhao et al., 2021a) and does not account for terrestrial biogenic INPs (Creamean et al., 2020) due to the lack of treatments in the model. In addition, both D15 and SM20 schemes cannot represent the high ice nucleating ability of HLD at warm temperatures at Zeppelin in summer 2016 (symbol "G" in Figure 8), which is attributed to soil organic matter by Tobo et al. (2019). When these organics are taken into account in the model, model overestimation for site G will get even worse, implying an overestimation of surface dust concentrations and/or HLD dust emission at Svalbard in the summertime. In summary, the model's INP biases in the Arctic are likely due to biases in the simulated aerosol fields (e.g., dust, MOA, and BC) and uncertainties in current ice nucleation parameterizations or missing representations of other INP sources (e.g., terrestrial biogenic aerosols).

In addition, we do not explicitly represent the potential ice nucleation ability differences in freshly emitted HLD and long-range transported LLD caused by the aging and the coatings of pollutants (Kulkarni et al., 2014; Boose et al., 2016). However, D15 and SM20 may already take the aging effect into account implicitly. Because D15 is based on the Saharan and Asian dust data collected over the Pacific Ocean basin and US Virgin Islands, respectively, which are far away from the corresponding LLD sources, while SM20 is derived from the freshly emitted Icelandic HLD, which is subjected to less aging effect.

The comparisons above are based on INP concentrations at a given temperature set by the INP instruments, which reflects the potential INP populations under ambient aerosol conditions. Next, we examine the immersion freezing rate of dust originating from the seven tagged sources (Figure 9) to evaluate the influences of HLD and LLD on ice nucleation processes in mixed-phase clouds. It is noted that the immersion freezing rate here is calculated online in the model using the ambient temperature and the default CNT ice nucleation parameterization.

Deleted: it is noted that
Deleted: chemical
Deleted: coating
Deleted: dust (
Deleted: includes
Deleted: are
Deleted: dust
Deleted: processes

Compared with its contribution to the dust burdens, the contribution of the HLD to the annual mean mixed-phase cloud immersion freezing rate is relatively small (~10% below 600 hPa) (Figure 9a). This is because the HLD is mainly located in the lower troposphere and not a lot of HLD can reach the mixed-phase cloud levels (or the freezing level), especially under the case that the HLD tends to be more prevalent in the warm seasons (see more discussion below). Among the LLD sources, North African dust (Figure 9c) and East Asian dust (Figure 9f) are the two major contributors, both of which are responsible for more than 20% of the annual mean immersion freezing rate in the mixed-phase clouds. Consistent with the vertical distribution of dust concentrations, the North African dust has its maximum contribution (30-40%) at around 500 hPa, while the East Asian dust plays a more important role at higher altitudes (above 400 hPa). Dust from Central Asia also has a moderate contribution (~20%) to the immersion freezing rate in the Arctic (Figure 9d).

Considering the different seasonality of HLD and LLD in the Arctic, we next investigate the seasonal variations of the immersion freezing rate in the Arctic mixed-phase clouds from HLD and two dominating LLD sources (NAf and EAs) (Figure 10). HLD has the largest contribution to the Arctic immersion freezing rate in boreal autumn, with more than 30% below 700 hPa and up to 50% near the surface (Figure 10c). It is related to the prevalence of HLD and relatively cold temperatures during this time in the Arctic. This is not the case for the summer, when the freezing level is relatively high. Although it is responsible for 50% of the total Arctic dust burden in the boreal summer, HLD has a limited contribution to the immersion freezing rate in the clouds (Figure 10b), because its weak vertical transport makes it hard to reach the freezing line. The contrast results in summer and autumn suggest that the immersion freezing rate in the Arctic clouds is influenced by air temperature in addition to the aerosols. It also implies that the surface INP

measurements may not reflect the complete picture of INP effects and more aircraft INP measurements are needed in the future. The seasonal variations of the immersion freezing rate from NAf and EAs are weaker than that from HLD but are still subjected to the vertical temperature change with season. The North African dust contributes more in spring and winter, while the East Asian dust is more important in summer and autumn.

3.4 Impact on cloud properties and radiative fluxes

Dust INPs can freeze the supercooled liquid droplets, which impacts the cloud microphysical and macrophysical properties and modulates the Earth's radiative balance. To examine such impacts, we conduct three sensitivity experiments that turn off the heterogeneous ice nucleation in the mixed-phase clouds by dust from Arctic local source, North Africa, and East Asia, respectively (i.e., noArc, noNAf, and noEAs in Table 1). The impacts of dust INPs from each source are determined by subtracting the respective sensitivity experiment from CTRL. Due to the feedbacks in dust emission and wet scavenging caused by changing cloud properties, the dust concentrations in the sensitivity experiments are not identical to CTRL, but the absolute differences are mostly within 5% (Figure S5 in the Supplement).

The cloud liquid and ice changes caused by dust INPs from each source are shown in Figure 11. Due to the strengthening of heterogeneous ice nucleation processes, INPs from all the three sources consistently reduce the total liquid mass mixing ratio (TLIQ) (Figure 11, first column) and cloud liquid droplet number concentration (NUMLIQ) (Figure 11, third column). The influence of HLD is mainly in the lower troposphere (Fig. 11, top row) and the influence of LLD extends to higher altitudes (Fig. 11, bottom two rows). Moreover, the cloud ice number concentration (NUMICE) decreases in the upper troposphere (Figure 11, fourth column), likely due to less cloud droplets available for the homogeneous freezing in cirrus cloud after introducing dust INPs in the mixed-

phase clouds. With fewer ice crystals falling from the cirrus clouds to the mixed-phase clouds, the WBF process in the mixed-phase clouds is inhibited (Figure S6). Other ice phase processes such as the accretion of cloud water by snow and the growth of ice crystals by vapor deposition also become less efficient, which decreases the total ice mass mixing ratio (TICE) above 600-700 hPa altitude (Figure 11, second column). TICE in the lower troposphere is increased because of immersion freezing and snow sedimentation from above.

Since liquid water path (LWP) is found to play a critical role in the Arctic radiative budget (e.g., Dong et al., 2010; Hofer et al., 2019; Shupe and Intrieri, 2004), we further investigate the seasonal variations of LWP changes caused by dust INPs from the three sources (Figure 12). Corroborated with their large contribution to the immersion freezing rate during this time (Figure 10, top row), HLD INPs produce the strongest LWP decrease (-1.3 g m^{-2}) in boreal autumn (Figure 12c), especially over North Canada and Greenland. The influence of LLD INPs on LWP peaks in spring and winter. North African dust tends to have a larger impact on North Eurasia, while East Asian dust impacts the west Arctic more.

Dust INPs from the three sources consistently increase (decrease) the annual mean downwelling shortwave (longwave) radiative flux (FSDS and FLDS) at the surface (Figure 13, left and middle columns). This is mainly due to the LWP decrease, which reduces the cloud albedo and longwave cloud emissivity. For HLD INPs, the FLDS reduction dominates over the FSDS increase and causes a net cooling effect at the Arctic surface (-0.24 W m^{-2}) (Figure 13c). In contrast, FSDS and FLDS changes related to the LLD INPs are comparable, which cancels each other and yields a small net radiative effect (0.08 W m^{-2} for NAf and -0.06 W m^{-2} for EAs) (Figure 13, bottom two rows). These differences in the net radiative effect are associated with different seasonalities of HLD and LLD. The insolation in the Arctic is strong in spring and summer but very limited in

autumn and winter. Since the HLD INPs have much stronger influence on LWP in autumn and winter than spring and summer (Figure 12), their contribution to the FSDS warming is weak and the FLDS cooling in autumn and winter dominates the annual mean effect (Table 4, part 1; also seen in Figure S7 to S9). LLD INPs are also important in spring and summer, so their FSDS warming effect is comparable to, and compensates for, the FLDS cooling effect.

We also examined the dust INP effect on cloud radiative forcing (CRF) at the top of the atmosphere (TOA) (Table 4, part 2). Dust INPs from the three sources induce a small net cooling (from -0.03 to -0.05 W m^{-2}) in the Arctic, with SW warming and LW cooling effects. The net cooling persists throughout the year, except for the summertime when the sufficient insolation results in a strong SW warming and, consequently, a net warming effect. Shi and Liu (2019) also found LLD can induce a generally net cooling effect above 70°N (0.18 to -1.95 W m^{-2}), but in a much higher magnitude than the sum of NAf and EAs dust INP effects (-0.15 W m^{-2} above 70°N, not shown in Table 4), which implies the aerosol glaciation effect on mixed-phase clouds is highly non-linear.

Finally, we evaluate the model performance in simulating the Arctic LWP and radiative fluxes against the Moderate Resolution Imaging Spectroradiometer (MODIS) LWP and the Cloud and the Earth's Radiant Energy System Energy Balanced and Filled Edition 4.1 (CERES-EBAF Ed4.1) products (Loeb et al., 2018; Kato et al., 2018), respectively (Figure 14). Two MODIS datasets are used, including the standard Collection 6.1 product (Pincus et al., 2012; P12) and Khanal et al. (2020; K20). The P12 product combines MODIS observations from Terra and Aqua and is designed for apples-to-apples comparisons with modelling results from the Cloud Feedback Model Intercomparison Project (CFMIP) Observation Simulator Package (COSP). The standard product has a well-known positive zonal bias near the poles that is strongly correlated with the solar zenith

Deleted: (Platnick et al., 2003)

Deleted: Platnick

Deleted: 2003; P03

Deleted: an improved one (

Deleted: .,

Deleted:) that corrected

Deleted: in

Deleted: Arctic in P03.

554 angle (SZA). The K20 product largely reduces this bias by utilizing the SZA and cloud
555 heterogeneity index in their retrieval algorithm. The MODIS simulator is used for to calculate the
556 simulated LWP. According to Fig. 14, the simulated LWP from the four experiments are lower
557 than P12 but higher than K20. All the four experiments also underestimate FSDS with too strong
558 SWCF and overestimate FLDS with too strong LWCF, which likely points to the biases of
559 modeled clouds (e.g., too much LWP as compared to K20). The differences among the model
560 experiments are very small compared to their discrepancies with observations. We notice including
561 dust INPs from the three sources decreases the simulated LWP (i.e., CTRL has less LWP than the
562 other experiments) (Figure 14a), which makes the model performance better if compared to K20.
563 Moreover, it shows noticeable improvements in simulating both surface and TOA radiative fluxes
564 after including dust INPs from each of the three sources (i.e., the results from CTRL are closer to
565 the CERES results than the other three experiments) (Figure 14b-e).
566 Overall, including HLD or LLD INPs do not contribute a lot to the reduction of biases in
567 simulating the LWP and radiative fluxes in the AMPCs. However, the representation of AMPCs
568 in global climate models is associated with multiple cloud macro- and microphysical processes,
569 and large-scale dynamics (Morrison et al., 2012) (see more discussion in Section 4), which interact
570 with one another non-linearly. Therefore, even though including HLD or LLD INPs do not
571 improve the representation of AMPCs significantly in our model, a good representation of dust
572 INPs, especially including HLD INPs, could still be of great importance for parameterizing
573 AMPCs in the model.

Deleted: comparison

Deleted: P03

4. Discussion

The HLD emission in our CTRL simulation is manually tuned up by 10 times to match the estimate by Bullard et al. (2016), which is derived by compiling field measurements in Iceland and Alaska. Since the instruments were operated under extreme Arctic conditions and the sampling is very scarce, this estimate may have large uncertainties. Therefore, the tuned HLD emission can be biased as well. Considering the overestimation of Greenland dust deposition, summertime surface dust concentrations at Alert station, and surface INP concentrations at Svalbald, our tuning may cause a regional and temporal high bias in HLD dust emissions. We examine this uncertainty by conducting a sensitivity experiment with halving HLD emissions in CTRL (i.e., HLD_half) and analysing the interannual variability of CTRL and HLD_half simulations (Table S2 and Figures S10-S11). The HLD_half simulation indeed has a better performance than CTRL. However, the high bias for Greenland deposition and the summertime overestimation of Alert dust surface concentration still exist, which reflects the limitation of the dust emission parameterization we use. This parameterization may not be able to capture the spatial distribution of dust emissions across the Arctic, considering that the model performance at other sites is much better (e.g., Heimaey, Figure 3a). Also, the HLD emissions and their regional distributions have large interannual variabilities. Therefore, as we mentioned in Section 3.1, comparing model simulations with measurements conducted in different years may result in large uncertainties.

Deleted:) is much better.

The overestimation of surface dust and INP concentrations may imply a too weak vertical transport of HLD, considering the low biases of dust in the upper troposphere as compared with ARCTAS measurements and CALIPSO retrievals. The weak vertical transport at the source regions in EAMv1 was also found in Wu et al. (2020), which was related to the too strong dry deposition at the surface layer. If this bias is addressed, HLD would contribute less (more) to the

Arctic dust concentrations in the lower (upper) troposphere, which suggests a larger contribution of HLD to the heterogeneous ice nucleation in the mixed-phase clouds in the summertime. As a result, the HLD would induce a more positive net downwelling radiative flux at the surface in summer and a less negative annual mean radiative effect. It is also noted that the underprediction in the upper troposphere dust may come from a weak long-range transport of LLD. If this is the case, the HLD would have a weaker contribution to the upper level dust concentrations and likely less of an impact on mixed-phase cloud heterogeneous ice nucleation in the summertime.

In addition, EAMv1 has intrinsic biases in its cloud microphysics parameterizations. As mentioned in Section 2.1, the WBF process rate in EAMv1 is tuned down by a factor of 10, which results in too many supercooled liquid clouds in high latitudes (Y. Zhang et al., 2019; M. Zhang et al., 2020). Shi and Liu (2019) found the sign and magnitude of dust INP cloud radiative effect in the Arctic would change, after removing the tuning factor for the WBF process in EAMv1. Moreover, EAMv1 does not account for several secondary ice production mechanisms, which are suggested to have a large impact on the ice crystal number concentrations and thus cloud phase (Zhao and Liu, 2021; Zhao et al., 2021b). All these uncertainties in the cloud microphysical processes would interact non-linearly and influence our estimate of INP radiative effect and should be addressed in future studies.

5. Conclusions

In this study, we investigate the source attribution of dust aerosols in the Arctic and quantify the relative importance of Arctic local dust versus long-range transported LLD to the Arctic dust loading and INP population. We found that HLD is responsible for 30.7% of the total dust burden in the Arctic, whereas LLD from Asia and North Africa contributes 44.2% and 24.2%, respectively.

The vertical transport of HLD is limited due to the stable cold air in the Arctic and thus it contributes more to the dust burden in the lower troposphere. In boreal summer and autumn when the contribution of HLD is at a maximum because of stronger local dust emissions, HLD is responsible for more than 30% of the Arctic dust loading below 800 hPa, but less than 10% above 700 hPa. In contrast, LLD from North African and East Asian dust dominates the dust burden in the free troposphere, since the poleward transport of LLD follows the uplifted isentropes. The North African and East Asian dust accounts for about two thirds of the dust loading above 700 hPa, with the remaining one third from other LLD sources. The North African dust contributes more between 500 and 700 hPa, while the East Asian dust dominates in the upper troposphere (above 400 hPa) because of its high emission heights. In addition, the North Africa source has a larger contribution in springtime, while the other three seasons are more influenced by the East Asian source.

Modeled dust INP concentrations are investigated following three ice nucleation parameterizations: CNT, D15 and SM20. Compared with INP measurements, our results show that including HLD as INPs significantly improves the model performance in simulating Arctic INP concentrations, especially for the ground measurements and for the measurements conducted in summer and autumn. We also examine the INP contributions from BC and SSA based on Sc20 and M18, respectively. The model suggests that both of them are only weak sources compared with dust. We note that the model may underestimate SSA INPs and currently misses the representation of terrestrial biological INPs. The model biases of INPs can also be due to bias in simulating Arctic dust concentrations and/or the uncertainties in ice nucleation parameterizations.

We examine the contribution of dust from the three sources (Arctic, North Africa, and East Asia) to the ambient immersion freezing rate in the Arctic. The contribution from HLD shows a strong

Deleted: two

seasonal variation, with the peak contribution in boreal autumn (above 20% below 500 hPa). In summer, although HLD has strong contributions to the dust loading and INP concentrations in the lower troposphere, its impact on the ambient immersion freezing rate is limited due to the warm temperatures and weak vertical transport. This finding implies that surface INP measurements may not be sufficient in representing the INP population in the Arctic mixed-phase clouds and more measurements of INP vertical profiles are needed in the future. North African and East Asian dust are the two major LLD contributors to the ambient immersion freezing rate. The annual mean contribution (30-40%) from North African dust peaks at around 500 hPa, while the immersion freezing is dominated by East Asian dust (more than 40%) in the upper troposphere (above 400 hPa).

The cloud glaciation effects of dust INPs from local Arctic sources, and North African and East Asian sources, are further examined. It is found that INPs from all the three sources consistently result in a reduction in TLIQ and NUMLIQ. TICE and NUMICE at higher altitude also decrease, likely due to the weakening of homogeneous freezing in cirrus clouds. LWP reduction caused by HLD INPs is evident in autumn and winter, while those by dust INPs from the two LLD sources peak in spring. HLD INPs also drive a net cooling effect of -0.24 W m^{-2} in the downwelling radiative flux at the surface in the Arctic, while the net radiative effects of the two LLD INP sources are relatively small (0.08 W m^{-2} for NAf and -0.06 W m^{-2} for EAs). This variation in radiative effect reflects the seasonal difference between HLD and LLD. Our results also suggest that all the three dust sources result in a weak negative net cloud radiative effect (-0.03 to -0.05 W m^{-2}) in the Arctic, which is consistent with Shi and Liu (2019).

Overall, our study shows that the Arctic local dust, which has been overlooked in previous studies, may have large contributions to the Arctic dust loading and INP population. It can also

Deleted: effect

Deleted: is

influence the Arctic mixed-phase cloud properties by acting as INPs. Considering the climate impacts of local Arctic dust emissions will be important given a warming climate, where reduction in snow coverage and more exposure of dryland in the Arctic may lead to increased HLD emissions.

Code availability. The E3SM code is available on GitHub: https://github.com/E3SM-Project/E3SM.git.

Author contribution. YS and XL conceived the project. YS modified the code, conducted the simulations, and led the analyses with suggestions from XL, MW, XZ, ZK, and HB. XL supervised the study. YS wrote the first draft of the paper. All coauthors were involved in helpful discussions and revised the paper.

Competing interests. The authors declare that they have no conflict of interest.

Acknowledgements. The authors would like to thank Kang Yang and Dr. Zhien Wang for providing the CALIPSO dust extinction retrievals and Drs. Meng Zhang and Sarah Brooks for their comments and suggestions. Mingxuan Wu is supported by the US Department of Energy (DOE), Office of Biological and Environmental Researsch, Earth and Environmental System Modeling program as part of the Energy Exascale Earth System Model (E3SM) project. The Pacific Northwest National Laboratory (PNNL) is operated for DOE by the Battelle Memorial Institute under contract DE-AC05-76RLO1830. This research used resources of the National Energy

Commented [SY1]: Kang Yang and Prof. Wang for CALIPSO

Research Scientific Computing Center, a DOE Office of Science User Facility supported by the Office of Science of the U.S. Department of Energy under contract DE-AC02-05CH11231.

Financial support. This research was supported by the DOE Atmospheric System Research (ASR) Program (grants DE-SC0020510 and DE-SC0021211).

References

Albani, S., Mahowald, N. M., Perry, A. T., Scanza, R. A., Zender, C. S., Heavens, N. G., Maggi, V., Kok, J. F., and Otto-Bliesner, B. L.: Improved dust representation in the Community Atmosphere Model, J. Adv. Model. Earth Syst., 6, 541–570, https://doi.org/10.1002/2013MS000279, 2014.

Arimoto, R., Duce, R. A., Ray, B. J., Ellis Jr, W. G., Cullen, J. D., and Merrill, J. T.: Trace elements in the atmosphere over the North Atlantic, J. Geophys. Res. Atmos., 100(D1), 1199–1213, https://doi.org/10.1029/94JD02618, 1995.

Arnalds, O., Dagsson-Waldhauserova, P., and Olafsson, H.: The Icelandic volcanic aeolian environment: Processes and impacts — A review, Aeolian Res., 20, 176–195, https://doi.org/10.1016/j.aeolia.2016.01.004, 2016.

Atkinson, J. D., Murray, B. J., Woodhouse, M. T., Whale, T. F., Baustian, K. J., Carslaw, K. S., Dobbie, S., O'Sullivan, D., and Malkin, T. L.: The importance of feldspar for ice nucleation by mineral dust in mixed-phase clouds, Nature, 498, 355–358, https://doi.org/10.1038/nature12278, 2013.

Baddock, M. C., Mockford, T., Bullard, J. E., and Thorsteinsson, T.: Pathways of high-latitude dust in the North Atlantic, Earth Planet. Sci. Lett., 459, 170–182, https://doi.org/10.1016/j.epsl.2016.11.034, 2017.

de Boer, G., Morrison, H., Shupe, M. D., and Hildner, R.: Evidence of liquid dependent ice nucleation in high-latitude stratiform clouds from surface remote sensors, Geophys. Res. Lett., 38, L01803, https://doi.org/10.1029/2010GL046016, 2011.

Bogenschutz, P. A., Gettelman, A., Morrison, H., Larson, V. E., Craig, C., and Schanen, D. P.: Higher-order turbulence closure and its impact on climate simulations in the community atmosphere model, J. Clim., 26, 9655–9676, https://doi.org/10.1175/JCLI-D-13-00075.1, 2013.

Boose, Y., Sierau, B., García, M. I., Rodríguez, S., Alastuey, A., Linke, C., Schnaiter, M., Kupiszewski, P., Kanji, Z. A., and Lohmann, U.: Ice nucleating particles in the Saharan Air Layer, Atmos. Chem. Phys., 16, 9067–9087, https://doi.org/10.5194/acp-16-9067-2016, 2016.

Moved (insertion) [1]

Formatted: Font color: Black

719 Bory, A. J.-M., Biscaye, P. E., Svensson, A., and Grousset, F. E.: Seasonal variability in the origin
720 of recent atmospheric mineral dust at NorthGRIP, Greenland, Earth Planet. Sci. Lett., 196, 123–
721 134, https://doi.org/10.1016/S0012-821X(01)00609-4, 2002.

722 Bory, A. J.-M., Biscaye, P. E., and Grousset, F. E.: Two distinct seasonal Asian source regions for
723 mineral dust deposited in Greenland (NorthGRIP), Geophys. Res. Lett., 30,
724 https://doi.org/10.1029/2002GL016446, 2003.

725 Breider, T. J., Mickley, L. J., Jacob, D. J., Wang, Q., Fisher, J. A., Chang, R. Y.-W., and Alexander,
726 B.: Annual distributions and sources of Arctic aerosol components, aerosol optical depth, and
727 aerosol absorption, J. Geophys. Res. Atmos., 119, 4107–4124,
728 https://doi.org/10.1002/2013JD020996, 2014.

729 Bullard, J. E.: The distribution and biogeochemical importance of high-latitude dust in the Arctic
730 and Southern Ocean-Antarctic regions, J. Geophys. Res. Atmos., 122, 3098–3103,
731 https://doi.org/10.1002/2016JD026363, 2017.

732 Bullard, J. E. and Austin, M. J.: Dust generation on a proglacial floodplain, West Greenland,
733 Aeolian Res., 3, 43–54, https://doi.org/10.1016/j.aeolia.2011.01.002, 2011.

734 Bullard, J. E., Baddock, M., Bradwell, T., Crusius, J., Darlington, E., Gaiero, D., Gassó, S.,
735 Gisladottir, G., Hodgkins, R., McCulloch, R., McKenna-Neuman, C., Mockford, T., Stewart, H.,
736 and Thorsteinsson, T.: High-latitude dust in the Earth system, Rev. Geophys., 54, 447–485,
737 https://doi.org/10.1002/2016RG000518, 2016.

738 Creamean, J. M., Kirpes, R. M., Pratt, K. A., Spada, N. J., Maahn, M., de Boer, G., Schnell, R. C.,
739 and China, S.: Marine and terrestrial influences on ice nucleating particles during continuous
740 springtime measurements in an Arctic oilfield location, Atmos. Chem. Phys., 18, 18023–18042,
741 https://doi.org/10.5194/acp-18-18023-2018, 2018.

742 Creamean, J. M., Hill, T. C. J., DeMott, P. J., Uetake, J., Kreidenweis, S., and Douglas, T. A.:
743 Thawing permafrost: an overlooked source of seeds for Arctic cloud formation, Environ. Res. Lett.,
744 15, 084022, https://doi.org/10.1088/1748-9326/ab87d3, 2020.

745 Crusius, J., Schroth, A. W., Gassó, S., Moy, C. M., Levy, R. C., and Gatica, M.: Glacial flour dust
746 storms in the Gulf of Alaska: Hydrologic and meteorological controls and their importance as a
747 source of bioavailable iron, Geophys. Res. Lett., 38, L06602,
748 https://doi.org/10.1029/2010GL046573, 2011.

749 Dagsson-Waldhauserova, P., Arnalds, O., and Olafsson, H.: Long-term variability of dust events
750 in Iceland (1949–2011), Atmos. Chem. Phys., 14, 13411–13422, https://doi.org/10.5194/acp-14-
751 13411-2014, 2014.

752 DeMott, P. J., Sassen, K., Poellot, M. R., Baumgardner, D., Rogers, D. C., Brooks, S. D., Prenni,
753 A. J., and Kreidenweis, S. M.: African dust aerosols as atmospheric ice nuclei, Geophys. Res. Lett.,
754 30(14), 1732, https://doi.org/10.1029/2003GL017410, 2003.

DeMott, P. J., Prenni, A. J., Liu, X., Kreidenweis, S. M., Petters, M. D., Twohy, C. H., Richardson, M. S., Eidhammer, T., and Rogers, D. C.: Predicting global atmospheric ice nuclei distributions and their impacts on climate, Proc. Natl. Acad. Sci. U.S.A., 107(25), 11217–11222, https://doi.org/10.1073/pnas.0910818107, 2010.

DeMott, P. J., Prenni, A. J., McMeeking, G. R., Sullivan, R. C., Petters, M. D., Tobo, Y., Niemand, M., Möhler, O., Snider, J. R., Wang, Z., and Kreidenweis, S. M.: Integrating laboratory and field data to quantify the immersion freezing ice nucleation activity of mineral dust particles, Atmos. Chem. Phys., 15, 393–409, https://doi.org/10.5194/acp-15-393-2015, 2015.

Dong, X., Xi, B., Crosby, K., Long, C. N., Stone, R. S., and Shupe, M. D.: A 10 year climatology of Arctic cloud fraction and radiative forcing at Barrow, Alaska, J. Geophys. Res. Atmos., 115, D17212, https://doi.org/10.1029/2009JD013489, 2010.

Dörnbrack, A., Stachlewska, I. S., Ritter, C., and Neuber, R.: Aerosol distribution around Svalbard during intense easterly winds, Atmos. Chem. Phys., 10, 1473–1490, https://doi.org/10.5194/acp-10-1473-2010, 2010.

Fenn, R. W. and Weickmann, H. K.: Some results of aerosol measurements, Geofisica Pura e Applicata, 42, 53–61, https://doi.org/10.1007/BF02113389, 1959.

Gettelman, A. and Morrison, H.: Advanced two-moment bulk microphysics for global models. Part I: off-line tests and comparison with other schemes, J. Clim., 28, 1268–1287, https://doi.org/10.1175/JCLI-D-14-00102.1, 2015.

Ghan, S. J. and Zaveri, R. A.: Parameterization of optical properties for hydrated internally mixed aerosol, J. Geophys. Res., 112, D10201, https://doi.org/10.1029/2006JD007927, 2007.

Ginoux, P., Chin, M., Tegen, I., Prospero, J. M., Holben, B., Dubovik, O., and Lin, S.-J.: Sources and distributions of dust aerosols simulated with the GOCART model, J. Geophys. Res., 106, 20255–20273, https://doi.org/10.1029/2000JD000053, 2001.

Golaz, J.-C., Larson, V. E., and Cotton, W. R.: A PDF-based model for boundary layer clouds. Part I: Method and model description, J. Atmos. Sci., 59, 3540-3551, https://doi.org/10.1175/1520-0469(2002)059<3540:APBMFB>2.0.CO;2, 2002.

Groot Zwaaftink, C. D., Grythe, H., Skov, H., and Stohl, A.: Substantial contribution of northern high-latitude sources to mineral dust in the Arctic, J. Geophys. Res. Atmos., 121, 13678-13697, https://doi.org/10.1002/2016JD025482, 2016.

Hiranuma, N., Brooks, S. D., Moffet, R. C., Glen, A., Laskin, A., Gilles, M. K.m Liu, P., Macdonald, A. M., Strapp, J. W., McFarquhar, G. M: Chemical characterization of individual particles and residuals of cloud droplets and ice crystals collected on board research aircraft in the ISDAC 2008 study, J. Geophys. Res. Atmos., 118, 6564-6579, https://doi.org/10.1002/jgrd.50484, 2013.

790 Hofer, S., Tedstone, A. J., Fettweis, X., and Bamber, J. L.: Cloud microphysics and circulation
791 anomalies control differences in future Greenland melt, Nat. Clim. Chang., 9, 523–528,
792 https://doi.org/10.1038/s41558-019-0507-8, 2019.

793 Holben, B. N., Eck, T. F., Slutsker, I., Tanré, D., Buis, J. P., Setzer, A., Vermote, E., Reagan, J.
794 A., Kaufman, Y. J., Nakajima, T., Lavenu, F., Jankowiak, I., and Smirnov, A.: AERONET—A
795 Federated Instrument Network and Data Archive for Aerosol Characterization, Remote Sens.
796 Environ., 66, 1–16, https://doi.org/10.1016/S0034-4257(98)00031-5, 1998.

797 Hoose, C. and Möhler, O.: Heterogeneous ice nucleation on atmospheric aerosols: a review of
798 results from laboratory experiments, Atmos. Chem. Phys., 12, 9817–9854,
799 https://doi.org/10.5194/acp-12-9817-2012, 2012.

800 Huang, Z., Huang, J., Hayasaka, T., Wang, S., Zhou, T., and Jin, H.: Short-cut transport path for
801 Asian dust directly to the Arctic: a case study, Environ. Res. Lett., 10, 114018,
802 https://doi.org/10.1088/1748-9326/10/11/114018, 2015.

803 Huneeus, N., Schulz, M., Balkanski, Y., Griesfeller, J., Prospero, J., Kinne, S., Bauer, S., Boucher,
804 O., Chin, M., Dentener, F., Diehl, T., Easter, R., Fillmore, D., Ghan, S., Ginoux, P., Grini, A.,
805 Horowitz, L., Koch, D., Krol, M. C., Landing, W., Liu, X., Mahowald, N., Miller, R., Morcrette,
806 J.-J., Myhre, G., Penner, J., Perlwitz, J., Stier, P., Takemura, T., and Zender, C. S.: Global dust
807 model intercomparison in AeroCom phase I, Atmos. Chem. Phys., 11, 7781–7816,
808 https://doi.org/10.5194/acp-11-7781-2011, 2011.

809 Irish, V. E., Hanna, S. J., Willis, M. D., China, S., Thomas, J. L., Wentzell, J. J. B., Cirisan, A., Si,
810 M., Leaitch, W. R., Murphy, J. G., Abbatt, J. P. D., Laskin, A., Girard, E., and Bertram, A. K.: Ice
811 nucleating particles in the marine boundary layer in the Canadian Arctic during summer 2014,
812 Atmos. Chem. Phys., 19, 1027–1039, https://doi.org/10.5194/acp-19-1027-2019, 2019.

813 Jacob, D. J., Crawford, J. H., Maring, H., Clarke, A. D., Dibb, J. E., Emmons, L. K., Ferrare, R.
814 A., Hostetler, C. A., Russell, P. B., Singh, H. B., Thompson, A. M., Shaw, G. E., McCauley, E.,
815 Pederson, J. R., and Fisher, J. A.: The Arctic Research of the Composition of the Troposphere
816 from Aircraft and Satellites (ARCTAS) mission: design, execution, and first results, Atmos. Chem.
817 Phys., 10, 5191–5212, https://doi.org/10.5194/acp-10-5191-2010, 2010.

818 Kato, S., Rose, F. G., Rutan, D. A., Thorsen, T. E., Loeb, N. G., Doelling, D. R., Huang, X., Smith,
819 W. L., Su, W., and Ham, S.-H.: Surface irradiances of Edition 4.0 Clouds and the Earth's Radiant
820 Energy System (CERES) Energy Balanced and Filled (EBAF) data product, J. Climate, 31, 4501-
821 4527, https://doi.org/10.1175/JCLI-D-17-0523.1, 2018.

822 Khanal, S., Wang, Z., and French, J. R.: Improving middle and high latitude cloud liquid water
823 path measurements from MODIS, Atmos. Res., 243. 105033.
824 https://doi.org/10.1016/j.atmosres.2020.105033, 2020.

825 Kinne, S., Schulz, M., Textor, C., Guibert, S., Balkanski, Y., Bauer, S. E., Berntsen, T., Berglen,
826 T. F., Boucher, O., Chin, M., Collins, W., Dentener, F., Diehl, T., Easter, R., Feichter, J., Fillmore,
827 D., Ghan, S., Ginoux, P., Gong, S., Grini, A., Hendricks, J., Herzog, M., Horowitz, L., Isaksen, I.,
828 Iversen, T., Kirkevåg, A., Kloster, S., Koch, D., Kristjansson, J. E., Krol, M., Lauer, A., Lamarque,

J. F., Lesins, G., Liu, X., Lohmann, U., Montanaro, V., Myhre, G., Penner, J., Pitari, G., Reddy, S., Seland, O., Stier, P., Takemura, T., and Tie, X.: An AeroCom initial assessment – optical properties in aerosol component modules of global models, Atmos. Chem. Phys., 6, 1815–1834, https://doi.org/10.5194/acp-6-1815-2006, 2006.

Kohfeld, K. E. and Harrison, S. P.: DIRTMAP: the geological record of dust, Earth-Sci. Rev., 54, 81–114, https://doi.org/10.1016/S0012-8252(01)00042-3, 2001.

Kok, J. F.: A scaling theory for the size distribution of emitted dust aerosols suggests climate models underestimate the size of the global dust cycle, Proc. Natl. Acad. Sci. U.S.A., 108(3), 1016–1021, https://doi.org/10.1073/pnas.1014798108, 2011.

Kok, J. F., Mahowald, N. M., Fratini, G., Gillies, J. A., Ishizuka, M., Leys, J. F., Mikami, M., Park, M.-S., Park, S.-U., Van Pelt, R. S., and Zobeck, T. M.: An improved dust emission model – Part 1: Model description and comparison against measurements, Atmos. Chem. Phys., 14, 13023–13041, https://doi.org/10.5194/acp-14-13023-2014, 2014a.

Kok, J. F., Albani, S., Mahowald, N. M., and Ward, D. S.: An improved dust emission model – Part 2: Evaluation in the Community Earth System Model, with implications for the use of dust source functions, Atmos. Chem. Phys., 14, 13043–13061, https://doi.org/10.5194/acp-14-13043-2014, 2014b.

Kok, J. F., Ridley, D. A., Zhou, Q., Miller, R. L., Zhao, C., Heald, C. L., Ward, D. S., Albani, S., and Haustein, K.: Smaller desert dust cooling effect estimated from analysis of dust size and abundance, Nat. Geosci., 10, 274–278, https://doi.org/10.1038/ngeo2912, 2017.

Kulkarni, G., Sanders, C., Zhang, K., Liu, X., and Zhao, C.: Ice nucleation of bare and sulfuric acid-coated mineral dust particles and implication for cloud properties, 119, 9993–10011, https://doi.org/10.1002/2014JD021567, 2014.

Larson, V. E., Golaz, J.-C., and Cotton, W. R.: Small-Scale and Mesoscale Variability in Cloudy Boundary Layers: Joint Probability Density Functions, J. Atmos. Sci., 59, 3519-3539, https://doi.org/10.1175/1520-0469(2002)059<3519:SSAMVI>2.0.CO;2, 2002.

Liu, X., Xie, S., Boyle, J., Klein, S. A., Shi, X., Wang, Z., Lin, W., Ghan, S. J., Earle, M., Liu, P. S. K., and Zelenyuk, A.: Testing cloud microphysics parameterizations in NCAR CAM5 with ISDAC and M-PACE observations, J. Geophys. Res., 116, D00T11, https://doi.org/10.1029/2011JD015889, 2011.

Liu, X., Ma, P.-L., Wang, H., Tilmes, S., Singh, B., Easter, R. C., Ghan, S. J., and Rasch, P. J.: Description and evaluation of a new four-mode version of the Modal Aerosol Module (MAM4) within version 5.3 of the Community Atmosphere Model, Geosci. Model Dev., 9, 505–522, https://doi.org/10.5194/gmd-9-505-2016, 2016.

Loeb, N. G., Doelling, D. R., Wang, H., Su, W., Nguyen, C., Corbett, J. G., Liang, L., Mitrescu, C., Rose, F. G., and Kato, S.: Clouds and the Earth's Radiant Energy System (CERES) Energy Balanced and Filled (EBAF) Top-of-Atmosphere (TOA) Edition-4.0 Data Product. J. Climate, 31, 895-918, https://doi.org/ 10.1175/JCLI-D-17-0208.1, 2018.

867 Luo, C., Mahowald, N. M., and Corral, J. del: Sensitivity study of meteorological parameters on
868 mineral aerosol mobilization, transport, and distribution, J. Geophys. Res., 108, 4447,
869 https://doi.org/10.1029/2003JD003483, 2003.

870 Luo, T., Wang, Z., Ferrare, R. A., Hostetler, C. A., Yuan, R., and Zhang, D.: Vertically resolved
871 separation of dust and other aerosol types by a new lidar depolarization method, Opt. Express, 23,
872 14095-14107, https://doi.org/10.1364/OE.23.014095, 2015a.

873 Luo, T., Wang, Z., Zhang, D., Liu, X., Wang, Y., and Yuan, R.: Global dust distribution from
874 improved thin dust layer detection using A-train satellite lidar observations, Geophys. Res. Lett.,
875 42, 620–628, https://doi.org/10.1002/2014GL062111, 2015b.

876 Maenhaut, W., Fernandez-Jimenez, M.-T., Rajta, I., Dubtsov, S., Meixner, F. X., Andreae, M. O.,
877 Torr, S., Hargrove, J. W., Chimanga, P., and Mlambo, J.: Long-term aerosol composi- tion
878 measruments and source apportionment at Rukomechi, Zim- babwe, J. Aerosol Sci., 31(Suppl. 1),
879 S469–S470, 2000a.

880 Maenhaut, W., Fernandez-Jimenez, M.-T., Vanderzalm, J. L., Hooper, B. M., Hooper, M. A., and
881 Tapper, N. J.: Aerosol com- position at Jabiru, Australia and impact of biomass burning, J. Aerosol
882 Sci., 31(Suppl. 1), S745–S746, 2000b.

883 Mahowald, N. M., Engelstaedter, S., Luo, C., Sealy, A., Artaxo, P., Benitez-Nelson, C., Bonnet,
884 S., Chen, Y., Chuang, P. Y., Cohen, D. D., Dulac, F., Herut, B., Johansen, A. M., Kubilay, N.,
885 Losno, R., Maenhaut, W., Paytan, A., Prospero, J. M., Shank, L. M., and Siefert, R. L.:
886 Atmospheric iron deposition: global distribution, variability, and human perturbations, Ann. Rev.
887 Mar. Sci., 1, 245–278, https://doi.org/10.1146/annurev.marine.010908.163727, 2009.

888 Mason, R. H., Si, M., Chou, C., Irish, V. E., Dickie, R., Elizondo, P., Wong, R., Brintnell, M.,
889 Elsasser, M., Lassar, W. M., Pierce, K. M., Leaitch, W. R., MacDonald, A. M., Platt, A., Toom-
890 Sauntry, D., Sarda-Estève, R., Schiller, C. L., Suski, K. J., Hill, T. C. J., Abbatt, J. P. D., Huffman,
891 J. A., DeMott, P. J., and Bertram, A. K.: Size-resolved measurements of ice-nucleating particles
892 at six locations in North America and one in Europe, Atmos. Chem. Phys., 16, 1637–1651,
893 https://doi.org/10.5194/acp-16-1637-2016, 2016.

894 McCluskey, C. S., Ovadnevaite, J., Rinaldi, M., Atkinson, J., Belosi, F., Ceburnis, D., Marullo, S.,
895 Hill, T. C. J., Lohmann, U., Kanji, Z. A., O'Dowd, C., Kreidenweis, S. M., and DeMott, P. J.:
896 Marine and terrestrial organic ice-nucleating particles in pristine marine to continentally
897 influenced Northeast Atlantic air masses, J. Geophys. Res. Atmos., 123, 6196–6212,
898 https://doi.org/10.1029/2017JD028033, 2018.

899 McFarquhar, G. M., Ghan, S., Verlinde, J., Korolev, A., Strapp, J. W., Schmid, B., Tomlinson, J.
900 M., Wolde, M., Brooks, S. D., Cziczo, D., Dubey, M. K., Fan, J., Flynn, C., Gultepe, I., Hubbe, J.,
901 Gilles, M. K., Laskin, A., Lawson, P., Leaitch, W. R., Liu, P., Liu, X., Lubin, D., Mazzoleni, C.,
902 Macdonald, A.-M., Moffet, R. C., Morrison, H., Ovchinnikov, M., Shupe, M. D., Turner, D. D.,
903 Xie, S., Zelenyuk, A., Bae, K., Freer, M., and Glen, A.: Indirect and Semi-direct Aerosol Campaign:
904 The Impact of Arctic Aerosols on Clouds, Bull. Amer. Meteor. Soc., 92, 183–201,
905 https://doi.org/10.1175/2010BAMS2935.1, 2011.

Morrison, H., de Boer, G., Feingold, G., Harrington, J., Shupe, M. D., and Sulia, K.: Resilience of persistent Arctic mixed-phase clouds, Nat. Geosci., 5, 11–17, https://doi.org/10.1038/ngeo1332, 2012.

Murray, B. J., O'Sullivan, D., Atkinson, J. D., and Webb, M. E.: Ice nucleation by particles immersed in supercooled cloud droplets, Chem. Soc. Rev., 41, 6519-6554, https://doi.org/10.1039/c2cs35200a, 2012.

Paramonov, M., David, R. O., Kretzschmar, R., and Kanji, Z. A.: A laboratory investigation of the ice nucleation efficiency of three types of mineral and soil dust, Atmos. Chem. Phys., 18, 16515–16536, https://doi.org/10.5194/acp-18-16515-2018, 2018.

Prenni, A. J., Harrington, J. Y., Tjernström, M., DeMott, P. J., Avramov, A., Long, C. N., Kreidenweis, S. M., Olsson, P. Q., and Verlinde, J.: Can ice-nucleating aerosols affect Arctic seasonal climate?, Bull. Amer. Meteor. Soc., 88, 541–550, https://doi.org/10.1175/BAMS-88-4-541, 2007.

Prenni, A. J., Demott, P. J., Rogers, D. C., Kreidenweis, S. M., Mcfarquhar, G. M., Zhang, G., and Poellot, M. R.: Ice nuclei characteristics from M-PACE and their relation to ice formation in clouds, Tellus B, 61, 436–448, https://doi.org/10.1111/j.1600-0889.2009.00415.x, 2009.

Prospero, J. M.: The Atmospheric Transport of Particles to the Ocean, in: Particle Flux in the Ocean, edited by: Ittekkot, V., Sch¨afer, P., Honjo, S., and Depetris, P. J., John Wiley & Sons Ltd., New York, 1996.

Prospero, J. M., Bullard, J. E., and Hodgkins, R.: High-Latitude Dust Over the North Atlantic: Inputs from Icelandic Proglacial Dust Storms, Science, 335, 1078–1082, https://doi.org/10.1126/science.1217447, 2012.

Prospero, J. M., Uematsu, M., and Savoie, D. L.: Mineral aerosol transport to the Pacific Ocean, edited by: Riley, J. P., 187–218, Academic Press, New York, 1989.

Rasch, P. J., Xie, S., Ma, P. -L., Lin, W., Wang, H., Tang, Q., Burrows, S. M., Caldwell, P., Zhang, K., Easter, R. C., Cameron-Smith, P., Singh, B., Wan, H., Golaz, J. -C., Harrop, B. E., Roesler, E., Bacmeister, J., Larson, V. E., Evans, K. J., Qian, Y., Taylor, M., Leung, L. R., Zhang, Y., Brent, L., Branstetter, M., Hannay, C., Mahajan, S., Mametjanov, A., Neale, R., Richter, J. H., Yoon, J. -H., Zender, C. S., Bader, D., Flanner, M., Foucar, J. G., Jacob, R., Keen, N., Klein, S. A., Liu, X., Salinger, A. G., Shrivastava, M., and Yang, Y.: An overview of the atmospheric component of the Energy Exascale Earth System Model, J. Adv. Model. Earth Syst., 11, 2377–2411, https://doi.org/10.1029/2019MS001629, 2019.

Ridley, D. A., Heald, C. L., Kok, J. F., and Zhao, C.: An observationally constrained estimate of global dust aerosol optical depth, Atmos. Chem. Phys., 16, 15097–15117, https://doi.org/10.5194/acp-16-15097-2016, 2016.

Sanchez-Marroquin, A., Arnalds, O., Baustian-Dorsi, K. J., Browse, J., Dagsson-Waldhauserova, P., Harrison, A. D., Maters, E. C., Pringle, K. J., Vergara-Temprado, J., Burke, I. T., McQuaid, J. B., Carslaw, K. S., and Murray, B. J.: Iceland is an episodic source of atmospheric ice-nucleating

Deleted: Platnick, S., King, M. D., Ackerman, S. A., Menzel, W. P., Baum, B…

Moved up [1]: . A.,

Deleted: Riédi, J. C., & Frey, R. A.: The MODIS cloud products: Algorithms and examples from terra, IEEE Trans. Geosci. Remote Sens., 41(2), 459-472. https://doi.org/10.1109/ TGRS.2002.808301¶

Formatted: Font color: Black

particles relevant for mixed-phase clouds, Sci. Adv., 6, eaba8137, https://doi.org/10.1126/sciadv.aba8137, 2020.

Schill, G. P., DeMott, P. J., Emerson, E. W., Rauker, A. M. C., Kodros, J. K., Suski, K. J., Hill, T. C. J., Levin, E. J. T., Pierce, J. R., Farmer, D. K., and Kreidenweis, S. M.: The contribution of black carbon to global ice nucleating particle concentrations relevant to mixed-phase clouds, Proc. Natl. Acad. Sci. U.S.A., 117, 22705–22711, https://doi.org/10.1073/pnas.2001674117, 2020.

Schweiger, A. J., Lindsay, R. W., Vavrus, S., and Francis, J. A.: Relationships between Arctic sea ice and clouds dusting autumn, J. Clim., 21, 4799-4810, https://doi.org/10.1175/2008JCLI2156.1

Shao, Y., Wyrwoll, K.-H., Chappell, A., Huang, J., Lin, Z., McTainsh, G. H., Mikami, M., Tanaka, T. Y., Wang, X., and Yoon, S.: Dust cycle: An emerging core theme in Earth system science, Aeolian Res., 2, 181–204, https://doi.org/10.1016/j.aeolia.2011.02.001, 2011.

Shi, Y. and Liu, X.: Dust Radiative Effects on Climate by Glaciating Mixed-Phase Clouds, Geophys. Res. Lett., 46, 6128–6137, https://doi.org/10.1029/2019GL082504, 2019.

Shupe, M. D. and Intrieri, J. M.: Cloud Radiative Forcing of the Arctic Surface: The Influence of Cloud Properties, Surface Albedo, and Solar Zenith Angle, J. Clim., 17, 616–628, https://doi.org/10.1175/1520-0442(2004)017<0616:CRFOTA>2.0.CO;2, 2004.

Si, M., Evoy, E., Yun, J., Xi, Y., Hanna, S. J., Chivulescu, A., Rawlings, K., Veber, D., Platt, A., Kunkel, D., Hoor, P., Sharma, S., Leaitch, W. R., and Bertram, A. K.: Concentrations, composition, and sources of ice-nucleating particles in the Canadian High Arctic during spring 2016, Atmos. Chem. Phys., 19, 3007–3024, https://doi.org/10.5194/acp-19-3007-2019, 2019.

Sirois, A., and Barrie, L. A.: Arctic lower tropospheric aerosol trends and composition at Alert, Canada: 1980-1995, J. Geophys. Res. Atmos., 104, 11599-11618, https://doi.org/10.1029/1999JD900077, 1999.

Smirnov, A., Holben, B. N., Eck, T. F., Dubovik, O., and Slutsker, I.: Cloud screening and quality control algorithms for the AERONET database, Remote Sens. Environ., 73, 337–349, https://doi.org/10.1016/S0034-4257(00)00109-7, 2000.

Stohl, A.: Characteristics of atmospheric transport into the Arctic troposphere, J. Geophys. Res., 111, D11306, https://doi.org/10.1029/2005JD006888, 2006.

Stone, R., Anderson, G., Andrews, E., Dutton, E., Harris, J., Shettle, E., Berk, A.: Asian dust signatures at Barrow: observed and simulated. Incursions and impact of Asian dust over Northern Alaska, Workshop on Remote Sensing of Atmospheric Aerosols, IEEE Workshop on Remote Sensing of Atmospheric Aerosols, 74-79, https://doi.org/10.1109/AERSOL.2005.1494152, 2005.

Tan, I. and Storelvmo, T.: Sensitivity study on the influence of cloud microphysical parameters on mixed-phase cloud thermodynamic phase partitioning in CAM5, J. Atmos. Sci., 73, 709-728, https://doi.org/10.1175/JAS-D-15-0152.1, 2016.

Tan, I. and Storelvmo, T.: Evidence of Strong Contributions from Mixed-Phase Clouds to Arctic Climate Change, Geophys. Res. Lett., 46, 2894–2902, https://doi.org/10.1029/2018GL081871, 2019.

Tanaka, T. Y. and Chiba, M.: A numerical study of the contributions of dust source regions to the global dust budget, Glob. Planet. Change, 52, 88–104, https://doi.org/10.1016/j.gloplacha.2006.02.002, 2006.

Tegen, I., Harrison, S. P., Kohfeld, K., Prentice, I. C., Coe, M., and Heimann, M.: Impact of vegetation and preferential source areas on global dust aerosol: Results from a model study, J. Geophys. Res. Atmos., 107, AAC 14-1-AAC 14-27, https://doi.org/10.1029/2001JD000963, 2002.

Tobo, Y., Adachi, K., DeMott, P. J., Hill, T. C. J., Hamilton, D. S., Mahowald, N. M., Nagatsuka, N., Ohata, S., Uetake, J., Kondo, Y., and Koike, M.: Glacially sourced dust as a potentially significant source of ice nucleating particles, Nat. Geosci., 12, 253–258, https://doi.org/10.1038/s41561-019-0314-x, 2019.

Vali, G.: Nucleation terminology, Bull. Am. Meteorol. Soc., 66, 1426–1427, 1985.

Vali, G., DeMott, P. J., Möhler, O., and Whale, T. F.: Technical Note: A proposal for ice nucleation terminology, Atmos. Chem. Phys., 15, 10263–10270, https://doi.org/10.5194/acp-15-10263-2015, 2015.

VanCuren, R. A., Cahill, T., Burkhart, J., Barnes, D., Zhao, Y., Perry, K., Cliff, S., and McConnell, J.: Aerosols and their sources at Summit Greenland – First results of continuous size- and time-resolved sampling, Atmos. Environ., 52, 82–97, https://doi.org/10.1016/j.atmosenv.2011.10.047, 2012.

Wang, H., Rasch, P. J., Easter, R. C., Singh, B., Zhang, R., Ma, P.-L., Qian, Y., Ghan, S. J., and Beagley, N.: Using an explicit emission tagging method in global modeling of source-receptor relationships for black carbon in the Arctic: Variations, sources, and transport pathways, J. Geophys. Res. Atmos., 119, 12888-12909, https://doi.org/10.1002/2014JD022297, 2014.

Wang, H., Easter, R. C., Zhang, R., Ma, P.-L., Singh, B., Zhang, K., Ganguly, D., Rasch, P. J., Burrows, S. M., Ghan, S. J., Lou, S., Qian, Y., Yang, Y., Feng, Y., Flanner, M., Leung, L. R., Liu, X., Shrivastava, M., Sun, J., Tang, Q., Xie, S., and Yoon, J.: Aerosols in the E3SM Version 1: New Developments and Their Impacts on Radiative Forcing, J. Adv. Model. Earth Syst., 12, e2019MS001851, https://doi.org/10.1029/2019MS001851, 2020.

Wang, Y., Liu, X., Hoose, C., and Wang, B.: Different contact angle distributions for heterogeneous ice nucleation in the Community Atmospheric Model version 5, Atmos. Chem. Phys., 14, 10411–10430, https://doi.org/10.5194/acp-14-10411-2014, 2014.

Westbrook, C. D. and Illingworth, A. J.: The formation of ice in a long-lived supercooled layer cloud: Ice Formation in Altocumulus, Q. J. R. Meteorol. Soc., 139, 2209–2221, https://doi.org/10.1002/qj.2096, 2013.

Wilson, T. W., Ladino, L. A., Alpert, P. A., Breckels, M. N., Brooks, I. M., Browse, J., Burrows, S. M., Carslaw, K. S., Huffman, J. A., Judd, C., Kilthau, W. P., Mason, R. H., McFiggans, G., Miller, L. A., Nájera, J. J., Polishchuk, E., Rae, S., Schiller, C. L., Si, M., Vergara-Temprado, J., Whale, T. F., Wong, J. P. S., Wurl, O., Yakobi-Hancock, J. D., Abbatt, J. P. D., Aller, J. Y., Bertram, A. K., Knopf, D. A., and Murray, B. J.: A marine biogenic source of atmospheric ice-nucleating particles, Nature, 525, 234–238, https://doi.org/10.1038/nature14986, 2015.

Winker, D. M., Tackett, J. L., Getzewich, B. J., Liu, Z., Vaughan, M. A., and Rogers, R. R.: The global 3-D distribution of tropospheric aerosols as characterized by CALIOP, Atmos. Chem. Phys., 13, 3345–3361, https://doi.org/10.5194/acp-13-3345-2013, 2013.

Wu, M., Liu, X., Yu, H., Wang, H., Shi, Y., Yang, K., Darmenov, A., Wu, C., Wang, Z., Luo, T., Feng, Y., and Ke, Z.: Understanding processes that control dust spatial distributions with global climate models and satellite observations, Atmos. Chem. Phys., 20, 13835–13855, https://doi.org/10.5194/acp-20-13835-2020, 2020.

Yang, K., Wang, Z., Luo, T., and Liu, X.: Upper Troposphere Dust Belt formation processes vary seasonally and spatially in the Northern Hemisphere, Commun. Earth Environ., accepted, 2022.

Yang, Y., Wang, H., Smith, S. J., Easter, R., Ma, P.-L., Qian, Y., Yu, H., Li, C., and Rasch, P. J.: Global source attribution of sulfate concentration and direct and indirect radiative forcing, Atmos. Chem. Phys., 17, 8903–8922, https://doi.org/10.5194/acp-17-8903-2017, 2017a.

Yang, Y., Wang, H., Smith, S. J., Ma, P.-L., and Rasch, P. J.: Source attribution of black carbon and its direct radiative forcing in China, Atmos. Chem. Phys., 17, 4319–4336, https://doi.org/10.5194/acp-17-4319-2017, 2017b.

Yang, Y., Wang, H., Smith, S. J., Zhang, R., Lou, S., Yu, H., Li, C., and Rasch, P. J.: Source Apportionments of Aerosols and Their Direct Radiative Forcing and Long-Term Trends Over Continental United States, Earth's Future, 6, 793–808, https://doi.org/10.1029/2018EF000859, 2018.

Zender, C. S., Bian, H., and Newman, D.: Mineral Dust Entrainment and Deposition (DEAD) model: Description and 1990s dust climatology, J. Geophys. Res., 108, 4416, https://doi.org/10.1029/2002JD002775, 2003.

Zhang, G. J. and McFarlane, N. A.: Sensitivity of climate simulations to the parameterization of cumulus convection in the Canadian climate centre general circulation model, Atmos.-Ocean, 33, 407–446, https://doi.org/10.1080/07055900.1995.9649539, 1995.

Zhang, K., Wan, H., Liu, X., Ghan, S. J., Kooperman, G. J., Ma, P.-L., Rasch, P. J., Neubauer, D., and Lohmann, U.: Technical Note: On the use of nudging for aerosol–climate model intercomparison studies, Atmos. Chem. Phys., 14, 8631–8645, https://doi.org/10.5194/acp-14-8631-2014, 2014.

Zhang, M., Liu, X., Diao, M., D'Alessandro, J. J., Wang, Y., Wu, C., Zhang, D., Wang, Z., and Xie, S.: Impacts of representing heterogeneous distribution of cloud liquid and ice on phase

partitioning of Arctic mixed-phase clouds with NCAR CAM5, J. Geophys. Res. Atmos., 124, 13071–13090, https://doi.org/10.1029/2019JD030502, 2019.

Zhang, M., Xie, S., Liu, X., Lin, W., Zhang, K., Ma, H.-Y., Zheng, X., and Zhang, Y.: Toward understanding the simulated phase partitioning of Arctic single-layer mixed-phase clouds in E3SM, Earth Space Sci., 7, e2020EA001125, https://doi.org/10.1029/2020EA001125, 2020.

Zhang, Y., Xie, S., Lin, W., Klein, S. A., Zelinka, M., Ma, P., Rasch, P. J., Qian, Y., Tang, Q., and Ma, H.: Evaluation of clouds in version 1 of the E3SM atmosphere model with satellite simulators, J. Adv. Model. Earth Syst., 11, 1253–1268, https://doi.org/10.1029/2018MS001562, 2019.

Zhao, X. and Liu, X.: Global Importance of Secondary Ice Production, Geophys. Res. Lett., 48, e2021GL092581, https://doi.org/10.1029/2021GL092581, 2021.

Zhao, X., Liu, X., Burrows, S. M., and Shi, Y.: Effects of marine organic aerosols as sources of immersion-mode ice-nucleating particles on high-latitude mixed-phase clouds, Atmos. Chem. Phys., 21, 2305–2327, https://doi.org/10.5194/acp-21-2305-2021, 2021a.

Zhao, X., Liu, X., Phillips, V. T. J., and Patade, S.: Impacts of secondary ice production on Arctic mixed-phase clouds based on ARM observations and CAM6 single-column model simulations, Atmos. Chem. Phys., 21, 5685–5703, https://doi.org/10.5194/acp-21-5685-2021, 2021b.

Table 1. Experiments conducted in this study.

Experiment	Description
CTRL	Control simulation using the CNT parameterization for heterogeneous ice nucleation and Kok et al. (2014a, b) for dust emission parameterization.
noArc	Same as CTRL, but turn off heterogeneous ice nucleation in mixed-phase clouds by HLD.
noNAf	Same as CTRL, but turn off heterogeneous ice nucleation in mixed-phase clouds by North African dust.
noEAs	Same as CTRL, but turn off heterogeneous ice nucleation in mixed-phase clouds by East Asian dust.

Table 2. Annual and seasonal mean Arctic (60-90°N) dust burden (mg m^{-2}) from different sources. The numbers in parentheses are the relative contributions (%) of each source to the total Arctic dust burden. The total Arctic dust burden is shown in the last row.

	ANN	MAM	JJA	SON	DJF
Arc	2.1 (30.7)	0.3 (3.9)	5.1 (50.4)	2.5 (47.5)	0.5 (14.6)
NAm	0.1 (0.9)	0.1 (1.3)	0.1 (0.6)	0.0 (0.7)	0.0 (1.2)
NAf	1.7 (24.2)	3.7 (41.4)	1.5 (14.4)	0.7 (12.9)	0.9 (26.4)
CAs	0.9 (12.8)	1.1 (12.5)	1.3 (13.0)	0.8 (14.7)	0.3 (10.1)
MSA	0.8 (11.5)	1.6 (17.9)	0.7 (7.0)	0.3 (6.1)	0.6 (17.4)
EAs	1.4 (19.9)	2.0 (23.0)	1.5 (14.7)	0.9 (18.1)	1.0 (30.2)
RoW	0.0 (0.0)	0.0 (0.0)	0.0 (0.0)	0.0 (0.0)	0.0 (0.1)
Total Burden (mg m^{-2})	6.9	8.9	10.2	5.2	3.3

1081 **Table 3.** Summary of the nine Arctic INP measurements used for INP comparisons in Figure 8.

	Location	Time period	Measured platform	Reference	Possible INP source mentioned in literature	INP source attribution from modeling[+]
A	Utqiaġvik	Apr. 2008 (spring)	Aircraft	McFarquhar et al. (2011)	Metallic or composed of dust[*]	LLD (EAs)
B	Alert	Mar. - May 2014 (spring)	Ground-based	Mason et al. (2016)	Not mentioned	LLD (EAs)
C	Alert	Mar. 2016 (spring)	Ground-based	Si et al. (2019)	LLD from Gobi Desert	LLD (EAs)
D	Zeppelin	Mar. 2017 (spring)	Ground-based	Tobo et al. (2019)	Marine organic aerosols	HLD (NEu)
E	Oliktok Point	Mar. - May 2017 (spring)	Ground-based	Creamean et al. (2018)	Dust and primary marine aerosols	LLD (mainly from EAs and some from NAf)
F	Alert	Jun. - Jul. 2014 (summer)	Ground-based	Mason et al. (2016)	Not mentioned	HLD (NCa)
G	Zeppelin	Jul. 2016 (summer)	Ground-based	Tobo et al. (2019)	HLD from Svalbard or other high latitude sources[**]	HLD (NEu)
H	Utqiaġvik	Oct. 2004 (autumn)	Aircraft	Prenni et al. (2007)	Dust and carbonaceous particles	HLD (NCa) and LLD (EAs)
I	South of Iceland	Oct. 2014 (autumn)	Aircraft	Sanchez-Marroquin et al. (2020)	Icelandic dust	Dominated by HLD (GrI), little from LLD (NAf)

1082 [+] The modeling analyses include INP contribution from HLD (using SM20), LLD (using D15),
1083 BC, and SSA. The
1084 [*] Carbonate, black carbon, and organic may also contribute, according to Hiranuma et al. (2013).
1085 [**] The HLD in this campaign is reported to have remarkably high ice nucleating ability, which may
1086 be related to the presence of organic matter.
1087

Table 4. Arctic (60-90°N) averaged surface downwelling radiative fluxes and TOA cloud radiative forcing changes caused by dust INPs originated from local Arctic sources (Arc), North Africa (NAf), and East Asia (EAs). Units are W m^{-2}.

	ANN			MAM			JJA			SON			DJF		
	SW	LW	Net	SW	LW	Net	SW	LW	Net	SW	LW	Net	SW	LW	Net
Part 1. INP effect on surface downwelling radiative fluxes															
Arc	0.11	-0.36	-0.24	0.27	-0.31	-0.03	0.12	0	0.12	0.04	-0.55	-0.51	0.02	-0.56	-0.54
NAf	0.33	-0.25	0.08	0.78	-0.60	0.19	0.50	0.01	0.51	0.02	-0.03	-0.02	0.03	-0.39	-0.36
EAs	0.35	-0.41	-0.06	0.68	-0.60	0.09	0.59	0.02	0.61	0.08	-0.27	-0.19	0.04	-0.80	-0.76
Part 2. INP effect on TOA cloud radiative forcing															
Arc	0.06	-0.11	-0.05	0.06	-0.07	-0.01	0.14	-0.02	0.12	0.03	-0.23	-0.20	0.01	-0.12	-0.11
NAf	0.20	-0.23	-0.03	0.34	-0.34	0	0.41	-0.18	0.24	0.03	-0.20	-0.16	0.02	-0.23	-0.21
EAs	0.20	-0.24	-0.04	0.22	-0.23	-0.02	0.46	-0.17	0.29	0.09	-0.29	-0.20	0.02	-0.26	-0.24

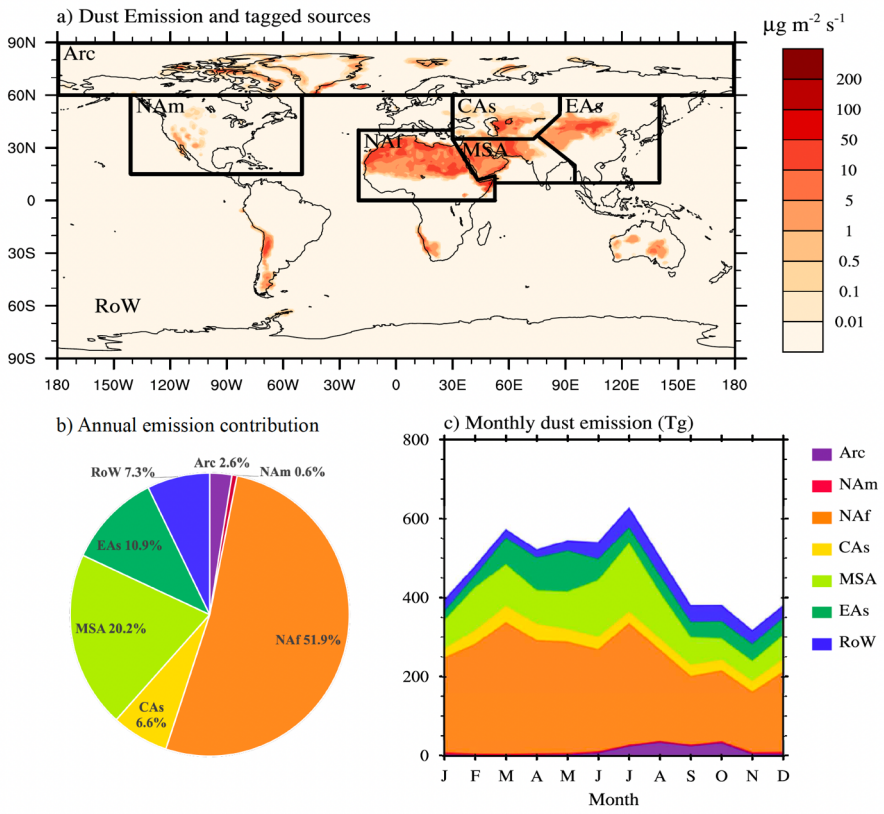

1092

1093 **Figure 1.** a) Simulated global annual mean dust emission with 7 tagged source regions (Arc:
1094 Arctic; NAm: North America; NAf: North Africa; CAs: Central Asia; MSA: Middle East and
1095 South Asia; EAs: East Asia; RoW: Rest of the World). b) The respective percentage contributions
1096 to the global annual mean dust emission from the individual source regions. c) Seasonal cycle of
1097 global dust emission.

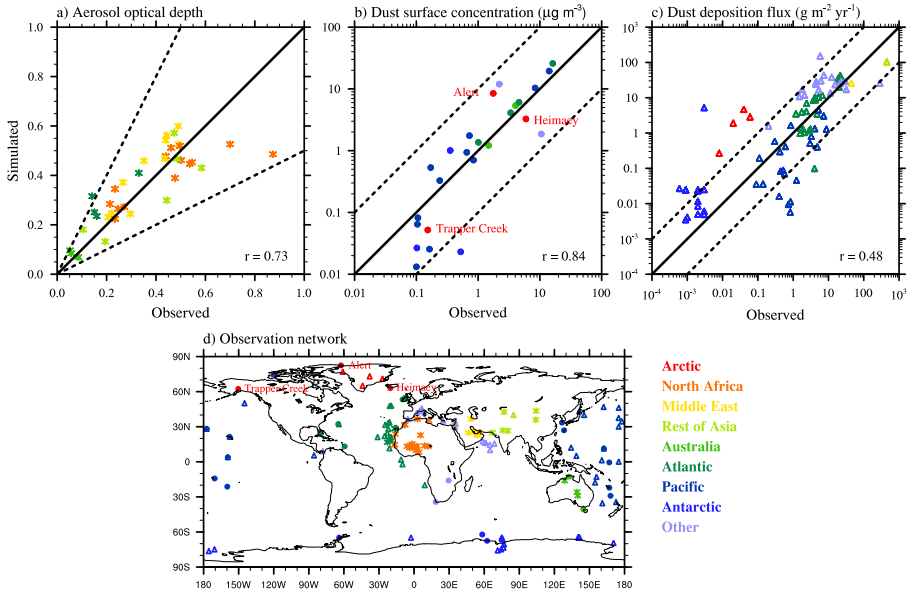

Figure 2. Comparison of observed and simulated a) averaged AOD at 40 dust-dominated stations (stars), b) dust surface concentration at 25 sites (circles), and c) dust deposition flux at 84 sites (triangles). Solid lines represent 1:1 comparison. Dashed lines mark 2 factor of magnitude bias in panel a) and 1 order of magnitude differences in panel b) and c). For each comparison, the correlation coefficient (r) is noted. The AOD data is conducted by AERONET. The dust surface concentration measurements include 20 stations managed by Rosenstiel School of Marine and Atmospheric Science at the University of Miami (Prospero et al., 1989; Prospero, 1996; Arimoto et al., 1995), two Australia stations (Maenhaut et al., 2000a, b), and three Arctic stations (Heimaey (Prospero et al., 2012), Alert (Sirois and Barrie, 1999), and Trapper Creek (IMPROVE)). The deposition fluxes data is a compilation of measurements from Ginoux et al. (2001), Mahowald et al. (2009), and the Dust Indicators and Records in Terrestrial and Marine Paleoenvironments (DIRTMAP) database (Tegen et al., 2002; Kohfeld and Harrison, 2001). Stations are grouped regionally and classified by different colors. The locations of the measurements are shown in panel d).

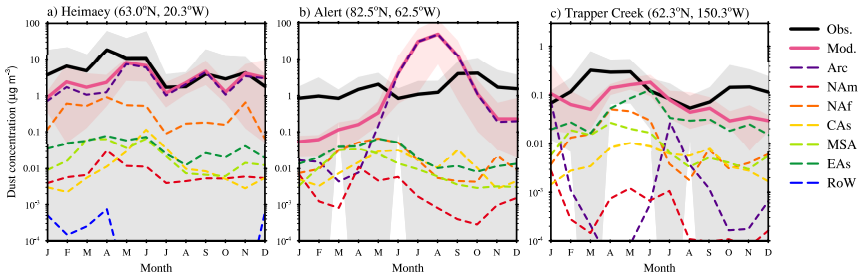

1114

1115 **Figure 3.** Comparison of measured (black solid line, with gray shade representing standard
1116 deviation) and simulated (pink solid line, with pink shade representing year-to-year variability)
1117 monthly mean dust surface concentration at three high latitude stations – a) Heimaey, b) Alert, and
1118 c) Trapper Creek. The model results are averaged from year 2007 to 2011. Contributions from
1119 seven tagged sources are shown by colored dashed lines. The locations of the three stations are
1120 shown in Figure 2d. The measurements at Heimaey (Prospero et al., 2012), Alert (Sirois and Barrie,
1121 1999), and Trapper Creek (IMPROVE) are averaged for the years 1997 to 2002, 1980 to 1995, and
1122 2007 to 2011, respectively. The dust concentrations at Trapper Creek only include particles with
1123 diameter less than 2.5 μm. The other two stations include dust over the whole size range.

1124

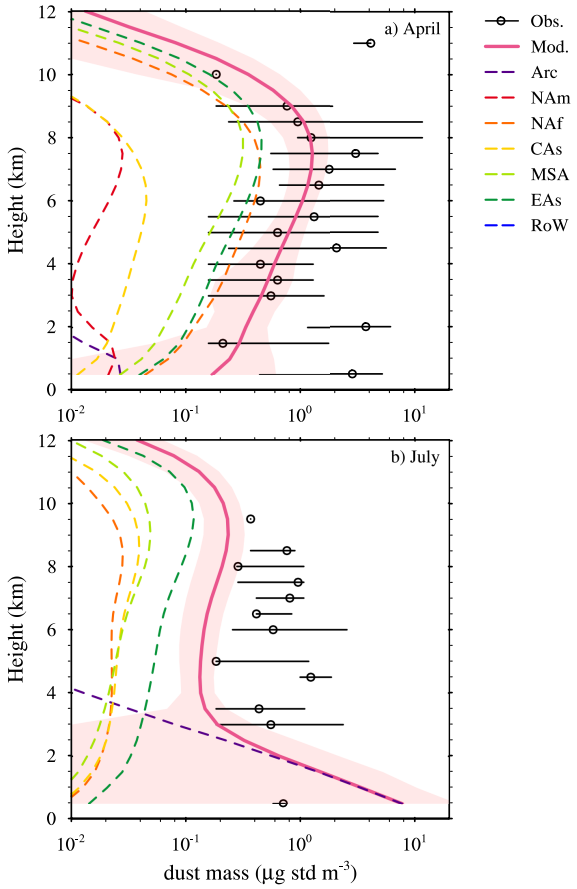

Figure 4. Comparison of vertical dust concentrations from ARCTAS flight observations (Jacob et al., 2010) (black circle) and CTRL simulation (pink solid line) in a) April and b) July. We show median values for observations at each level. The maximum and minimum of the measurements at each level are shown by black lines. Contributions from the seven tagged sources in CTRL are shown by colored dashed lines. The ARCTAS dust mass concentrations are derived from measured calcium and sodium concentrations. The measurements data are processed using the same method as Breider et al. (2020). Briefly, we assume a calcium to dust mass ratio of 6.8% and further correct the calcium concentrations for sea salt by assuming a calcium to sodium ratio of 4%. Only measurements obtained north of 60°N are used for the analyses. The low-altitude observations near Fairbanks, Barrow, and Prudhoe Bay are removed. Also, data from below 1 km on 1, 4, 5, 9

July is removed to exclude the influence of wildfire. The ARCTAS flight campaign was conducted in 2008, while the modeled vertical profiles are averaged for each April and July from 2007 to 2011, respectively. Following Groot Zwaaftink et al. (2016), the simulation profiles are averaged for the regions north of 60°N and 170°W to 35°W in April and 135°W to 35°W in July. Also, the observations have a cut-off size of 4 μm and thus is only compared with simulated dust concentrations in the same size range. The pink shade on each panel represents the standard deviation with respect to time and space for the simulated total dust concentrations.

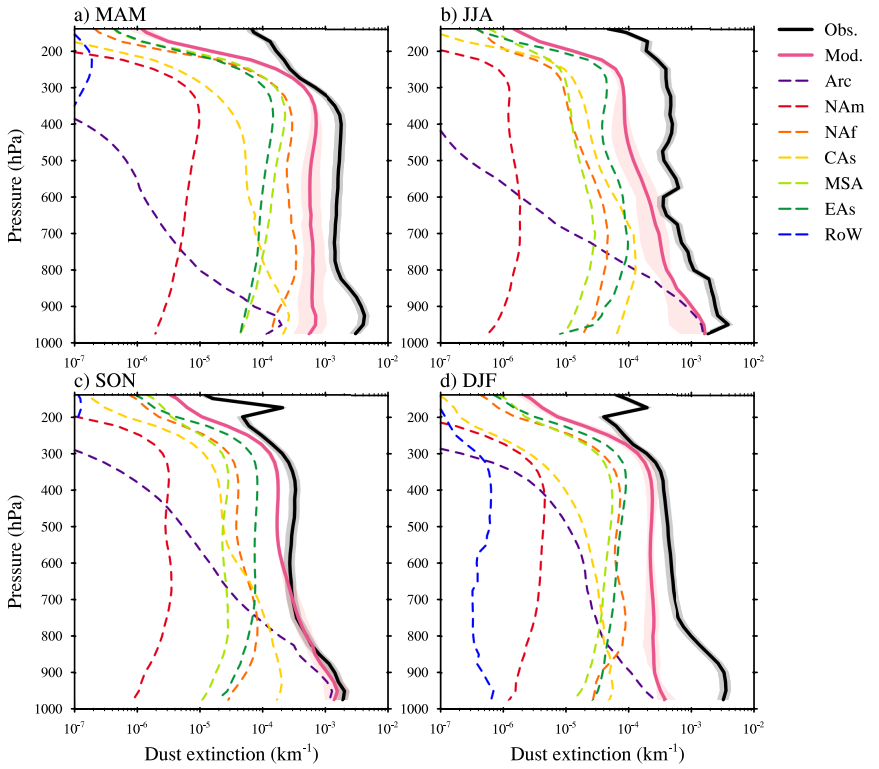

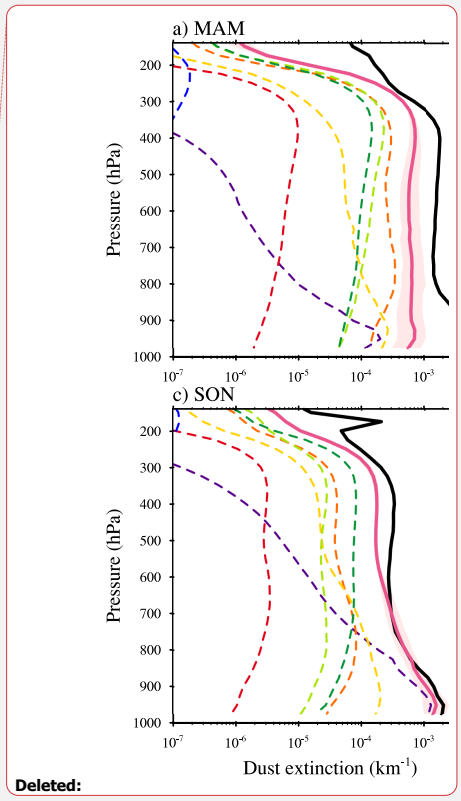

Figure 5. Comparison of seasonal CALIPSO retrieved (Luo et al., 2015a, b; Yang et al., 2022) (black solid line; with gray shade representing uncertainty) and model simulated (pink solid line; with pink shade representing year-to-year variability) dust extinction vertical profiles in the Arctic (above 60°N). Contributions from seven tagged sources are shown by colored dashed lines. The CALIPSO retrievals are for the year 2007 to 2009, while the model results are averaged over the same years. The uncertainties of the CALIPSO retrievals are assumed to be 20% following Yang et al. (2022).

Deleted: .

Deleted: retrieval is

Deleted: is

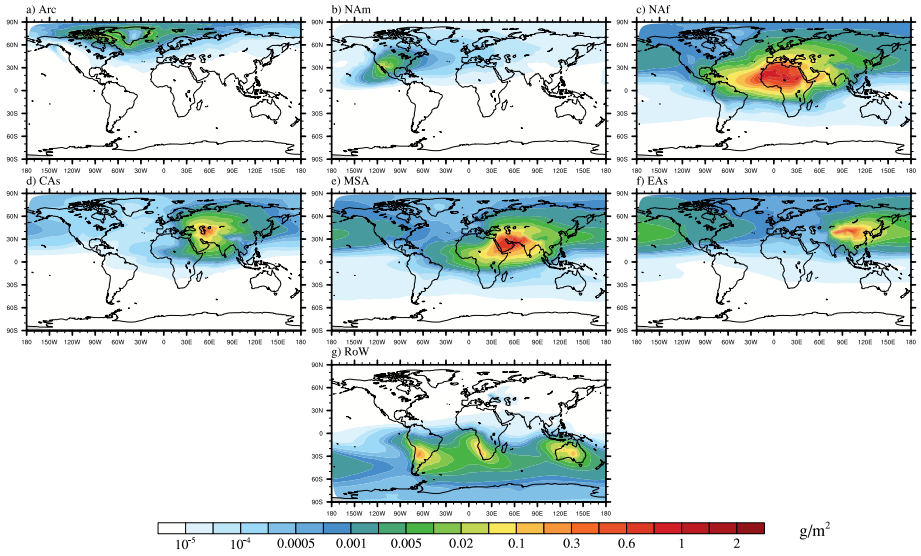

1156

1157 **Figure 6.** Spatial distribution of annual mean (year 2007 to 2011) dust column burdens for various
1158 tagged sources.

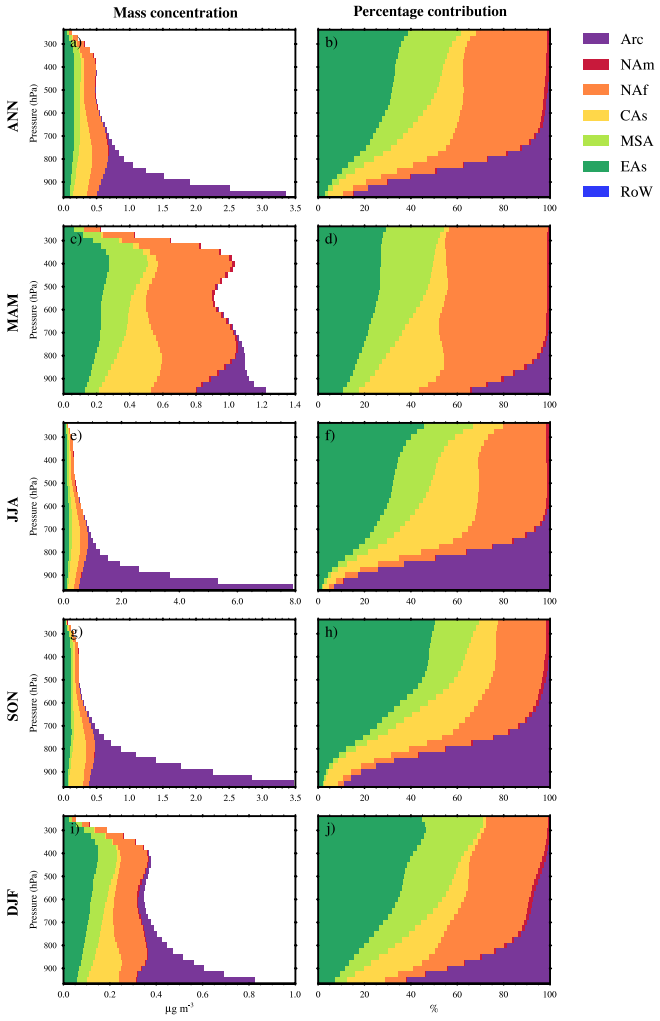

Figure 7. Annual and seasonal mean (year 2007 to 2011) Arctic (60-90°N) vertical dust concentrations (left panel) and percentage contributions from tagged sources (right panel). Different tagged sources are classified by different colors.

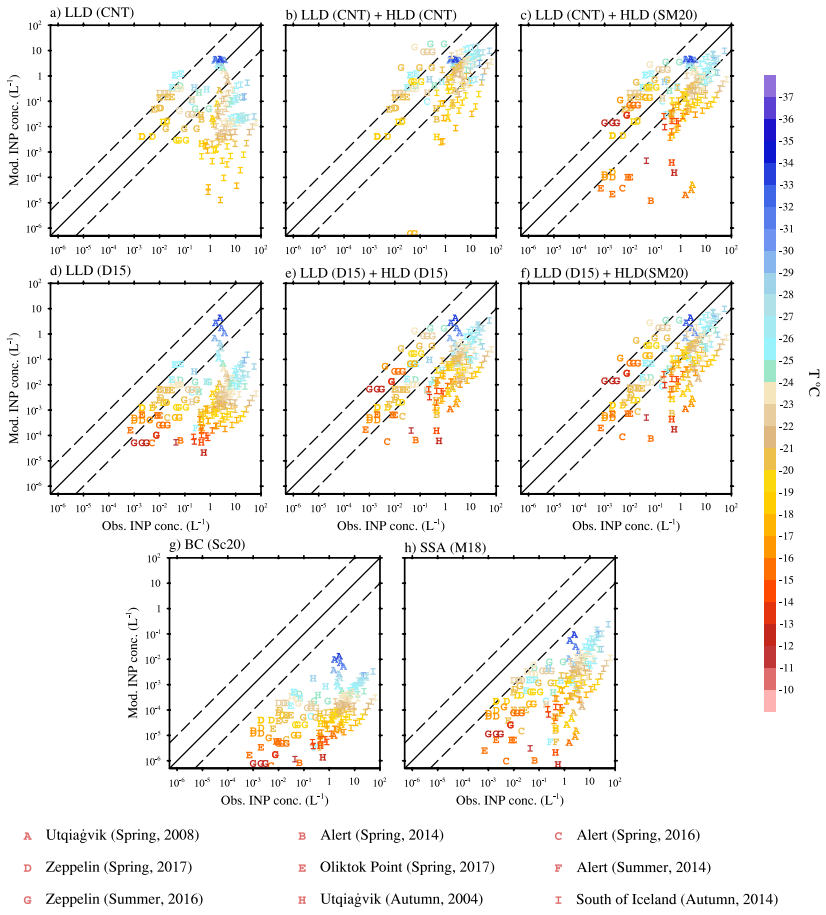

Figure 8. Comparison of predicted versus observed INP concentrations in the Arctic. The predicted INP concentrations are derived from a) LLD using classical nucleation theory (CNT), b) LLD and HLD, both using CNT, c) LLD using CNT and HLD using Sanchez-Marroquin et al (2020; SM20), c) LLD using DeMott et al. (2015; D15), d) LLD and HLD, both using D15, e) LLD using D15 and HLD using SM20, f) BC using Schill et al. (2020; Sc20), and g) SSA using McCluskey et al. (2018; M18). SSA includes both marine organic aerosol and sea salt. Nine INP datasets are classified by symbol "A" to "I", the color of which represents the temperature reported in the observations. The observations for datasets "A", "C", "E", "H" are monthly mean values. Samples for datasets "D", "G", "I" are selected randomly and only 15% of them are plotted. Details of each campaign are summarized in Table 3. The modelled INP concentrations are diagnosed

using the observed temperatures and monthly averaged aerosol properties of the corresponding month from year 2007 to 2011. The INP concentrations for CNT are defined as the CNT immersion freezing rate integrated by 10 s, following Hoose et al. (2010) and Wang et al. (2014). Solid line in each panel represents 1:1 comparison, while dashed lines outline one order of magnitude differences. The unit for INP concentration is L^{-1}.

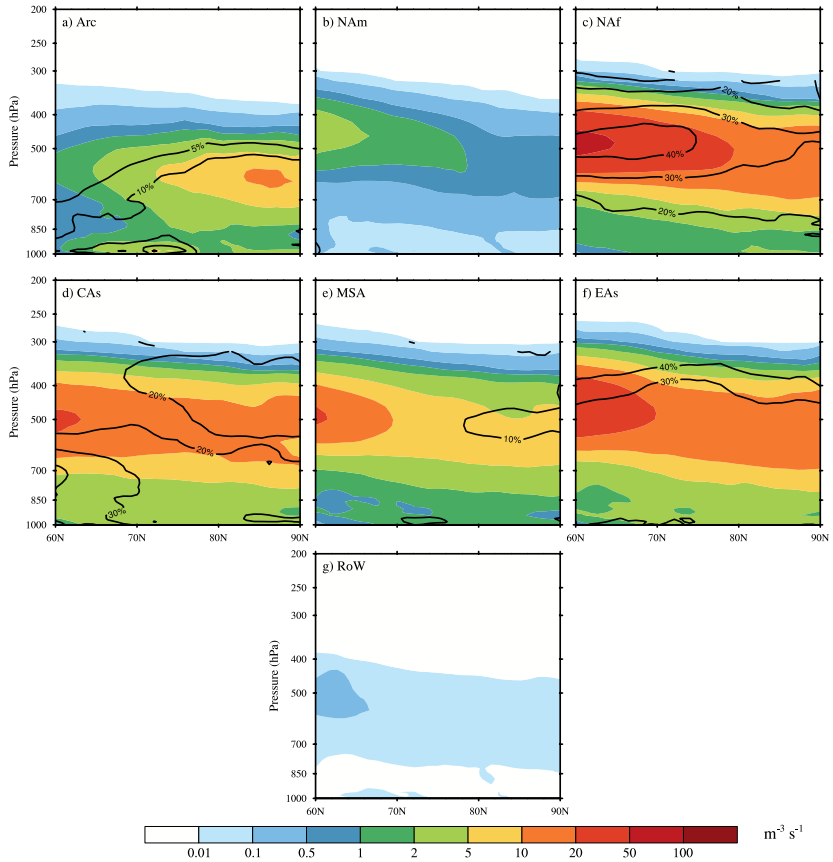

1180

1181 **Figure 9.** Annual and zonal mean (year 2007 to 2011) ambient mixed-phase cloud immersion
1182 freezing rates (unit: m^{-3} s^{-1}) in the Arctic for the seven dust sources. Black contours are the
1183 percentage contributions from each dust source to the total immersion freezing rate.

Deleted: (60-90°N)

1184

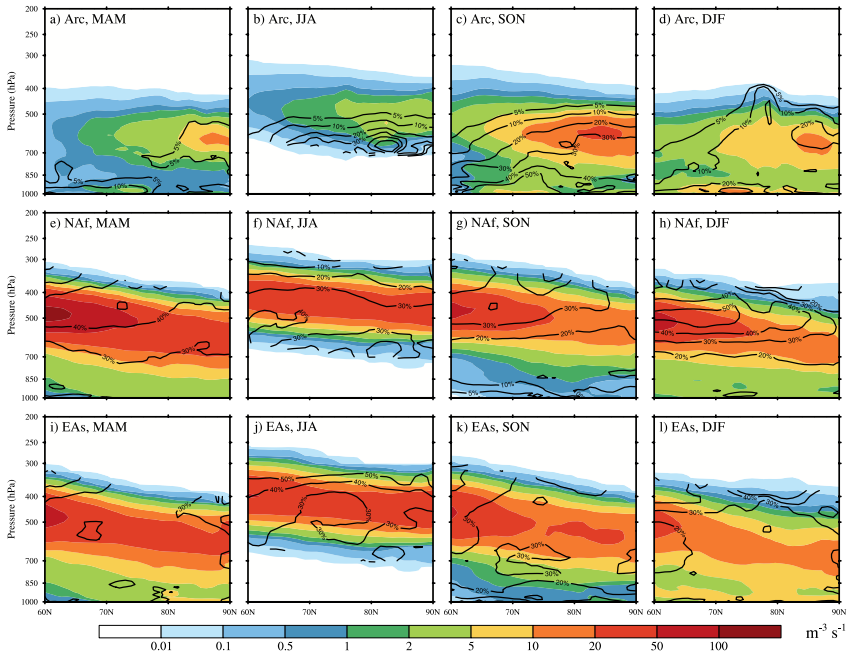

1186

1187 **Figure 10.** Seasonal variations (year 2007 to 2011) of the mixed-phase clouds immersion freezing
1188 rates (unit: m^{-3} s^{-1}) over the Arctic for dust emitted from the Arctic (top panel), North Africa
1189 (middle panel), and East Asia (bottom panel). Black contours are the percentage contributions
1190 from each dust source to the total immersion freezing rate in the corresponding season.

1191

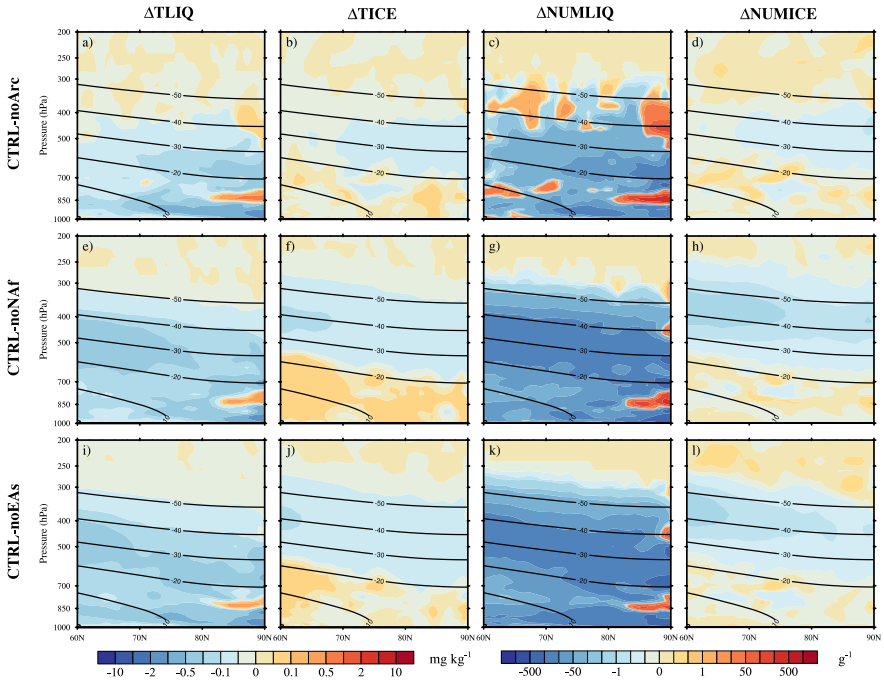

Figure 11. Annual and zonal mean differences (year 2007 to 2011) in total liquid water mass mixing ratio (TLIQ), total ice mixing ratio (TICE), cloud droplet number concentration (NUMLIQ), and cloud ice number concentration (NUMICE) in the Arctic. Black contours are zonal averaged temperatures in ºC. Top, middle, and bottom panels show the differences between CTRL and noArc, noNAf, and noEAs, respectively.

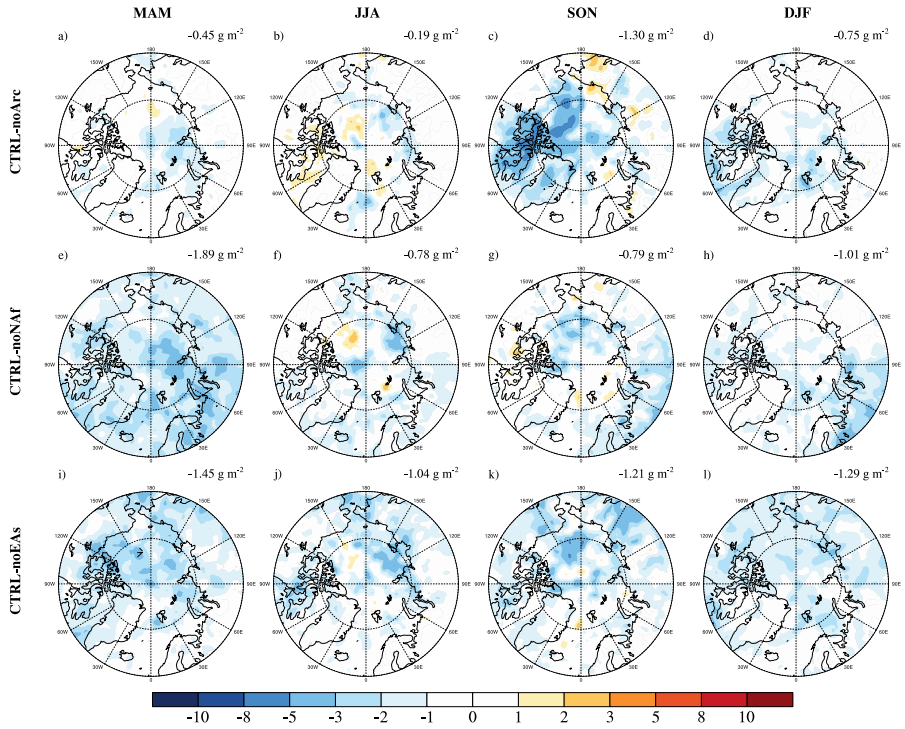

Figure 12. Seasonal changes (year 2007 to 2011) in LWP (unit: g m^{-2}) caused by dust INPs from the Arctic (top panel), North Africa (middle panel), and East Asia (bottom panel). The numbers are averaged LWP differences in the Arctic.

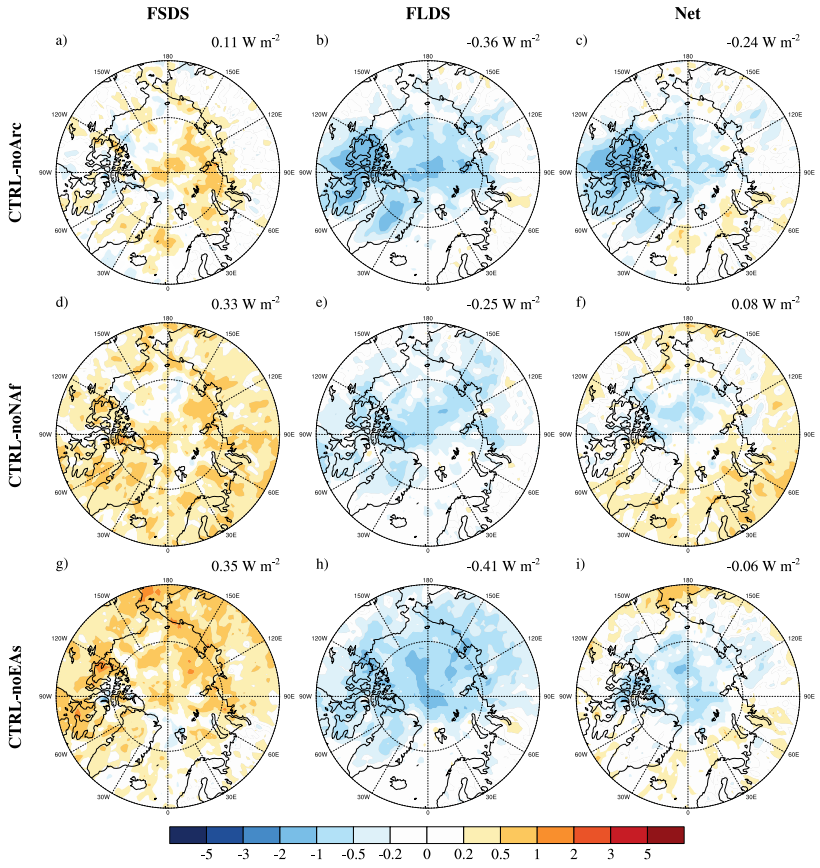

1203

1204 **Figure 13.** Changes in annual mean (year 2007 to 2011) downwelling radiative fluxes at the
1205 surface (unit: W m^{-2}) caused by dust INPs from the Arctic (top panel), North Africa (middle panel),
1206 and East Asia (bottom panel). Left, middle, and right panels are downwelling shortwave (FSDS),
1207 longwave (FLDS), and net (FSDS + FLDS) radiative fluxes, respectively. The numbers are
1208 averaged radiative flux differences in the Arctic.

1209

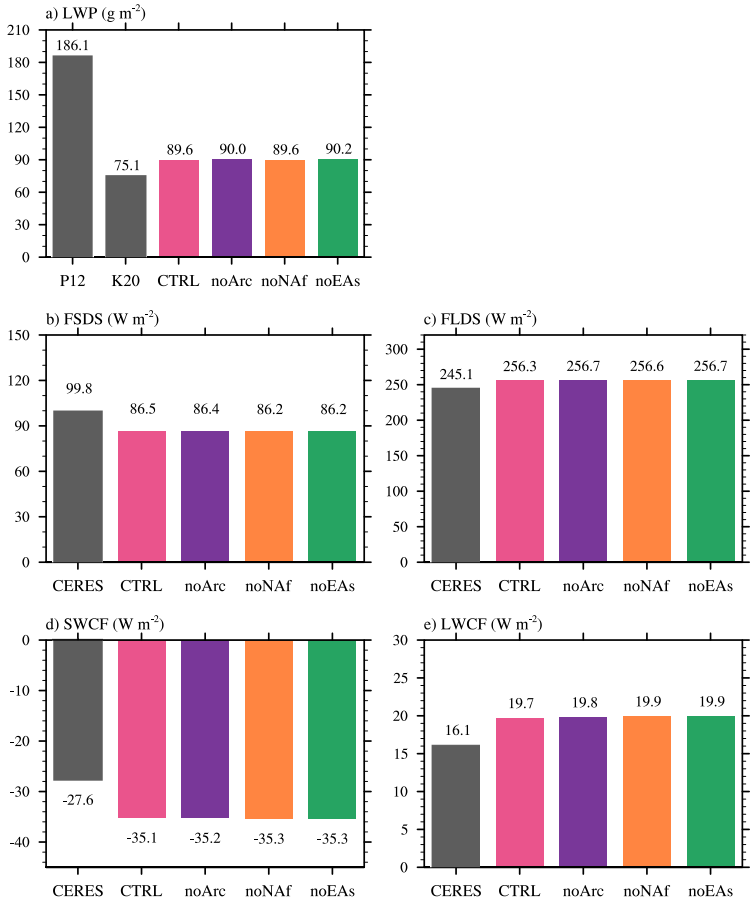

Figure 14. a) Annual mean Arctic (60°N to 80°N in this subplot) averaged LWP over ocean for the MODIS observations and the four simulations (2007-2008). Two MODIS datasets are used, including the standard product (Pincus et al., 2012; P12; averaged from 2007 to 2008) and an improved one (Khanal et al., 2020; K20; averaged from 2007 to 2009). The MODIS simulator is used to calculate the simulated LWP. b) - e) Annual mean Arctic (60°N to 90°N in these subplots) averaged b) FSDS, c) FLDS, d) SWCF, and e) LWCF for the CERES observation (2007-2011) and the four simulations (2007-2011).

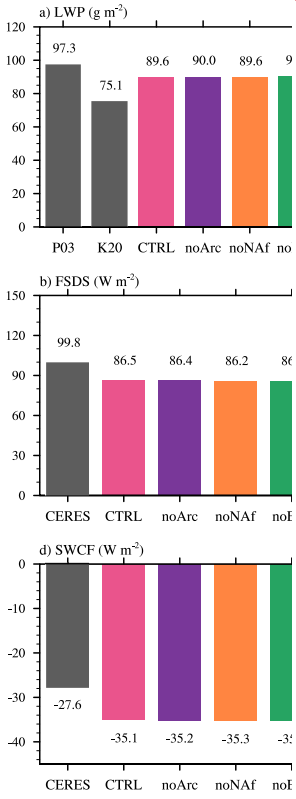

Deleted:

Deleted: (2007-2009)

Deleted: Platnick

Deleted: 2003; P03

Deleted:).